# The Design of a Fuzzy Sliding Mode Controller for CubeSat's Attitude Determination and Control System (ADCS)

*By: Salomon Zerihun*


ADDIS ABABA UNIVERSITY
ADDIS ABABA INSTITUTE OF TECHNOLOGY
MASTER OF SCIENCE IN CONTROL ENGINEERING

**Advisor:** Chala Merga (Assistant Professor)

Addis Ababa, Ethiopia
January 5, 2026

# ADDIS ABABA UNIVERSITY

ADDIS ABABA INSTITUTE OF TECHNOLOGY
SCHOOL OF ELECTRICAL AND COMPUTER ENGINEERING

MSc Thesis On:
The Design of a Fuzzy Sliding Mode Controller for CubeSat Attitude Determination and Control System (ADCS)

## Thesis Approval Sheet

Board of Examiners:

| | | |
|---|---|---|
| Dean, School of Graduate Committee | Signature | Date |
| _____ | _____ | _____ |
| Advisor: | Signature | Date |
| Chala Merga(Assistant Professor) | _____ | _____ |
| Internal Examiner | Signature | Date |
| Teshome Hambissa(PhD) |  | 05/01/2026 |
| External Examiner | Signature | Date |
| Getu Gabisa(PhD) | _____ | _____ |

# Declaration

I certify that I have never applied to this or any other institution for any other degree or certification, with the title "The Design of a Fuzzy Sliding Mode Controller for CubeSat's Attitude Determination and Control System (ADCS)" as part of the requirements for the Master of Science in Control Engineering degree under the Addis Ababa Institute of Technology's School of Electrical and Computer Engineering. Every the source of a material used in this thesis has been appropriately cited.

Salomon Zerihun

SIGNED: ..... DATE: 05/01/2026

# Acknowledgements

First of all, I feel obliged to give thanks to Almighty God for furnishing me with the fiber, occasion, and tolerance, as well as to a many individualities who helped me to finish this thesis. First and foremost, I want to unfeignedly thank to Dr. Chala Merga( PhD, Assistant Professor) for his enthusiastic supervision, superb advice, forbearance, and inestimable support during this exploration design. Thank you, for your helping with everything. Their perseverance and commitment are applaudable. To work with them is an enormous honor and I hope you have great success in both your particular and professional life. Furthermore, I want to a sincerely thank my parents and musketeers for their unwavering love, encouragement, and support. I'm grateful for the best, most enduring moral support and care have ever received, as well as for achieving my goal. At end of, I would want to sincerely thank everyone who helped me but whose names were with held.

# Abstract

This paper is about designing and analyzing a fuzzy sliding mode controller and its for the attitude determination and control system in CubeSats. CubeSat's being small and lightweight satellites, require robust and efficient attitude control to ensure proper orientation for mission critical operations such as communication, imaging, and power generation. Traditional Sliding Mode Control is well robustness against disturbances and uncertainties; however, it suffers from chattering, which can induce high oscillations and excessive wear on actuators. To address these challenges, this study integrates fuzzy logic with SMC to design a FSMC that mitigates chattering while preserving the robustness of the SMC. The proposed FSMC works fuzzy logic to dynamically adjust the sliding surface parameters and control gains, enhancing adaptability and reducing the negative impact of external disturbances.
The design process includes modeling CubeSat's rotational dynamics, developing sliding mode controller, and incorporating fuzzy rules to fine-tune the control actions. The performance of the FSMC is evaluated through simulations under various operating conditions, including different initial attitudes, external disturbances and Compare with PID Controller. Results demonstrate that the FSMC provides improved attitude control performance with reduced chattering, enhanced robustness, and better disturbance rejection capabilities compared to conventional control methods such as Compare with PID Controller. The FSMC is designed using a sliding mode control technique based on fuzzy logic, addressing challenges in nonlinear system stability. The sliding surface is design using error dynamics and a reference trajectory, providing a reliable control method. The FSMC mitigates the downsides of traditional sliding mode controllers by stabilizing the state trajectory on the sliding surface. The study concludes that the FSMC is effective solution for CubeSat attitude control, combining the benefits of fuzzy logic and sliding mode control to meet the stringent requirements of space missions.
**Keywords**: CubeSat, ADCS, Fuzzy Sliding Mode Controller (FSMC), Sliding Mode Control (SMC), Fuzzy Logic, PID

# List of Tables

**Table** **Page**

# List of Figures

**Figure** **Page**

# Table of Contents

# List of Acronyms

**ADCS**:Attitude Determination Control System
**ADS**:Attitude Determination System
**ACM**:Attitude Control Maneuver
**ACS**:Attitude Control System
**ANN**:Artificial Neural Network
**ANTIS**:Adaptive Euro Blurred Controller
**AOCS**:Attitude and Orbit Control System
**CG**:Center of Gravity
**ECI**:Earth Centered Inertial
**ECEF**:Earth Centered Earth Fixed
**FLC**:Fuzzy Logic Controller
**FOG**:Fiber Optic Gyroscopes
**FSMC**:Fuzzy Sliding Mode Controller
**GG**:Gravity Gradient
**IAE**:Integrated Absolute Error
**IFEHS**:Infrared Fixed Earth Horizon Sensor
**ISE**:Integrated Square Error
**ITSE**:Integrated Time Square Error
**ITAE**:Integrated Time Absolute Error
**LEO**:Low Earth Orbit
**LPV**:Linear Parameter-Varying
**LMI**:Linear Matrix Inequalities
**LQR**:Linear Quadratic Regulator
**MIMO**:Multi Input Multi Output
**MISO**:Multi Input Single Output
**NED**:North East Down
**NMPC**:Nonlinear Model Predictive Control
**PI**:Proportional Integral
**PID**:Proportional Integral Derivative
**PD**:Proportional Derivative
**PSO**:Particle Swarm Optimization
**SMC**:Sliding Mode Controller
**T2S**:Twisting Second Order Sliding Mode
**VSC**:Variable Structure Control
**SVD**:Singular Value Decomposition
**SISO**:Single Input Single Output

# Chapter 1

# Itroduction

The introduction in this Chapter represents; Background of study, Statements of Problem, Objectives, Significance, Scope, limitations, and Organization of Thesis.

## 1.1 Background of study

CubeSats are small artificial satellites composed of one or more 10cm cubes, typically launched as secondary payloads on larger rockets [1] and used for communication, technology demonstration, and Earth observation. Due to standardized interfaces, CubeSat awareness encourages low costs and rapid development times. The building block of the model, according to design specifications [2],[3], is a cube with a 10 cm edge length per side and a mass of approximately 1.3 kg. The high failure rate noted in initial missions is partly due to the lack of a top-level strategy in design and integration processes [4]. Orbital control has become a new challenge for many nanosatellites, although CubeSats have gained significant popularity [5]. CubeSats include several subsystems, notably the Attitude Determination and Control System (ADCS), which aims to manage chaotic trajectories in space. Fuzzy control techniques developed for ADCS can cancel chaotic behavior, enabling efficient spacecraft control. SMC to enhance nonlinear controller performance and is widely applied in robotic systems [6]. However, SMC suffers from high-frequency fluctuations due to the chattering phenomenon caused by the sign function [7]. Employing high switching gain to ensure efficiency may further strain control inputs and worsen chattering [8]. To improve ADCS performance, this thesis integrates both Fuzzy Logic Control (FLC) and SMC, addressing parametric uncertainty and disturbance rejection.

Sliding Mode Controller is recognized as robust control technique for satellite attitude control, maintaining stability under system uncertainties and disturbances. A saturation or approximate sign function to reduce chattering, though this may compromise precision[2] . Recent research incorporates fuzzy set theory into SMC to design Fuzzy Sliding Mode Controllers (FSMC), which reduce chattering and provide robust control [9],[8]. Based on spacecraft motion properties, an SMC law is proposed for attitude tracking, with Lyapunov theory ensuring system stability. The control process emphasizes reliable pointing and slewing missions for next-generation spacecraft [7]. Fuzzy logic is used to optimize sliding mode gain, further improving controller performance. Simulation results under unknown parameters and disturbances confirm the efficacy of the strategy against uncertainties. The ADCS integrates sensors, filters, estimators, and control algorithms, with actuators and sensor dynamics contributing to overall system behavior. FSMC design aims to eliminate chattering by replacing the switching variable **w** with a fuzzy inference system that approximates the sign function through smooth nonlinear mapping. Methods such as boundary layers, continuous control laws, gain tuning, and robustness against uncertainties are employed to reduce oscillations. The design of SMC improves tracking capability and ensures stability for satellite Euler angles (pitch, yaw, and roll). Nonlinear simulations with temporal delays and coupling effects demonstrate Lyapunov convergence to zero, confirming system stability. Classical proportional-derivative control leads to instability, whereas SMC successfully mitigates time-delay dynamics. In conclusion, this research illustrates how SMC enhances robustness and performance in nonlinear spacecraft control systems.

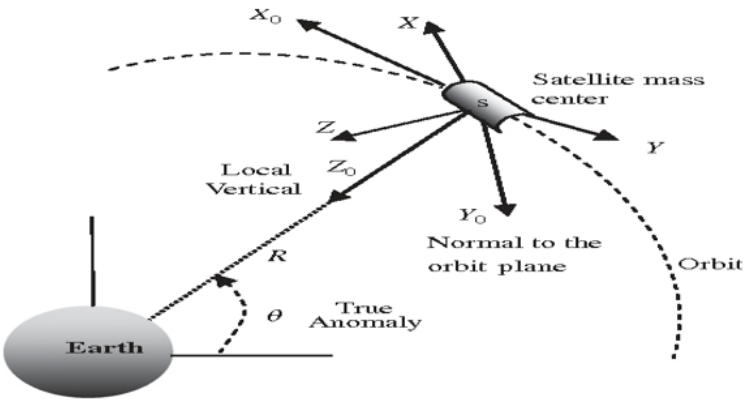


Figure 1.1: Body Reference Frames, Orbital Frames, and System Model [10]

## 1.2 Statements of Problem

Design of attitude is largely dependent on the Attitude Determination and Control System (ADCS). However, typical control techniques can struggle to precisely identify and manage attitudes due to uncertainties, non-linearity, and system disruptions. Probelem in design system that effectively addresses these issues by integrating fuzzy logic control and smc.It accurately evaluate the CubeSat's attitude parameters and send control signals while accounting for errors with disturbances in the system dynamics to control the satellite towards its desired attitude. The sensor measurements from gyroscopes, magnetometers, and other sensors to determine the CubeSat's attitude parameters, such as orientation and angular velocity.The proposed method should provide an accurate assessment of attitudes while compensating for measurement errors and noise.The integration of controller that regulate signals according to the expected attitude parameters. The controller must effectively handle uncertainties, non-linearity, disturbances, and a mathematical modelling the dynamics of plant, including rotational motion, external disturbances, and sensor measurements, to achieve stable attitude control. This model should represent the system's behavior accurately and serve as a basis for control system design and simulation.

Fuzzy SMC, along with attitude determination algorithms and mathematical models, will be implemented using MATLAB simulations. The solution to above problem yield a Fuzzy Sliding Mode Controller for ADCS based on CubeSat technology that can accurately assess and regulate the satellite's attitude by addressing uncertainties, non-linearity, and disturbances. Compared to traditional control techniques, the enhanced performance, robustness, and stability of this controller enable the CubeSat's attitude control system to operate more efficiently and reliably.Attitude determination is the process of ascertaining the satellite's orientation and angular velocity, whereas attitude control involves maintaining the appropriate orientation by applying necessary control inputs. SMC offers robustness against external disturbances and modeling uncertainties; however, it remains essential to manage uncertainties and non-linearity within the system.

## 1.3 Objectives

### 1.3.1 General Objective

The main objective of this thesis is to Design of a Fuzzy Sliding Mode Controller for CubeSat's Attitude Determination and Control System (ADCS) and to compare its performance with other controllers.

### 1.3.2 Specific Objectives

1. To design a sliding surface that can tolerate attitude dynamics, actuator failures, disruptions, and system uncertainties.
2. To approximate the nonlinear behavior of a CubeSat Attitude Determination and Control System (ADCS) using an inference system based on fuzzy logic.
3. To combine the sliding surface and fuzzy logic system to design a control law that ensures the CubeSat's attitude follows the reference attitude.
4. To use MATLAB for the mathematical modeling of the attitude dynamics of the CubeSat ADCS.
5. To utilize MATLAB-Simulink for the simulation and analysis of the proposed control strategy to determine its performance in attitude tracking.

## 1.4 Significance of Research Work

The research on the design of a fuzzy sliding mode controller for CubeSat's attitude determination and control system (ADCS) offers several significant advantages and prospects. It provides an appropriate platform for evaluating control systems and developing control technologies. Additionally, because the design and development of CubeSat systems can enhance theoretical lessons and offer students hands-on experience with satellite control systems, this research presents substantial opportunities for improving the educational process.The fuzzy sliding mode controller by offering a comprehensive range of tools for control system modeling and design. By leveraging MATLAB's powerful capabilities to efficiently simulate and assess control techniques, this integration enhances the research significantly.

Moreover, CubeSats may undertake increasingly complex missions such as deep space exploration or tasks requiring high-precision pointing and tracking if more robust and reliable control systems are developed for these small satellites. This advancement could greatly expand the reach and potential of CubeSat missions, opening new avenues for exploration and scientific research.The primary goal of this research is to improve the precision and effectiveness of attitude determination and control by focusing on the design of a fuzzy sliding mode controller. It is anticipated that this improvement will enhance the overall performance of CubeSat missions, increasing their likelihood of success and reliability in achieving mission objectives. In conclusion, this work offers significant educational and exploratory benefits while advancing the field of satellite control.

## 1.5 Scope of the Project

This research examines the existing body of knowledge about fuzzy control, sliding mode controllers, and CubeSat attitude determination control systems, including academic papers and technical resources. The design of the dynamics of satellite's attitude using mathematical modeling based on sensor measurements to estimate the CubeSat's attitude parameters. The algorithm must consider sensor integration to obtain precise estimates of the CubeSat's orientation and angular velocity.

The development of a Fuzzy Sliding Mode Controller (FSMC) will leverage computed attitude parameters to deliver control signals to the CubeSat's actuators. The FSMC will integrate both SMC and fuzzy control techniques to effectively handle uncertainties, non-linearity, and disturbances.Key design parameters include fuzzy logic rule definitions, sliding mode control laws, membership functions, and stability analysis. The control system will be evaluated through simulation and performance analysis using MATLAB software. Assessments will include stability analysis, robustness against uncertainties and disturbances, accuracy in attitude determination, and the ability to maintain desired attitudes. The reporting and documentation will compile analyses, simulation results, MATLAB/Simulink outputs, mathematical models, algorithms, and literature reviews. The documentation will be structured clearly and include relevant figures, explanations, and illustrations. A final report summarizing the thesis's methods, conclusions, and recommendations for further improvements will also be prepared.

## 1.6 Limitations of the Study

Despite the significant advancements offered by this study on the design of a fuzzy sliding mode controller for CubeSat's attitude determination and control system (ADCS), several limitations must be considered. The use of MATLAB-Simulink models may include assumptions and simplifications that do not fully capture the complexity of actual CubeSat dynamics. Such simplifications could impact the accuracy of simulation results, potentially overlooking factors like complex environmental disturbances, interactions with other satellite systems, and suboptimal actuator behavior.

Additionally, MATLAB's limitations may restrict the ability to perform extensive simulations for highly complex or large-scale scenarios. The design of the fuzzy logic system itself can be intricate and somewhat arbitrary, with the quality of the membership functions and rule sets significantly influencing the performance of the fuzzy sliding mode controller. Poor design choices during this phase may constrain the overall functionality of the controller. Furthermore, the FSMC developed in this research is specifically tailored to meet particular mission profiles and CubeSat specifications, which may limit its scalability and adaptability to different satellite designs or mission requirements.

## 1.7 Organization of the Thesis

This thesis is organized into six chapters, each addressing a different aspect of the topic.

1. Chapter 1: Introduces the concept of satellites and classifies their orbits based on altitude above the Earth, providing an overview of the thesis, including its objectives, statement of the problem, and scope of the research.
2. Chapter 2: Presents a literature survey of previous work on satellite attitude determination control systems.
3. Chapter 3: Formulates the detailed mathematical model of satellite dynamics and kinematics.
4. Chapter 4: Discusses the controller design based on the mathematical model to tackle the research problem.
5. Chapter 5: Focuses on simulation and discusses results obtained from the MATLAB/Simulink environment.
6. Chapter 6: Concludes the thesis and presents future work briefly.

# Chapter 2

# Literature Review

The many literature reviews on satellite attitude control are covered in this Chapter. One of the most important man-made objects that orbits earth or another body in space is satellite. It offers special benefits to human life, imaging, missile control, television signals, internet connections, forest monitoring, aviation, and ship tracking. In order to accomplish the intended attitude control of satellites, a number of academics from around globe have recently turned to controller algorithm, which has been extensively studied utilizing a variety of control techniques. Below is a discussion of a few of them:

An adaptive fuzzy SMC was created by Y. Li, X. Wang, and H. Zhang. [11] and is used to stabilize the attitude of flexible satellites. The three-axis attitude has been separately controlled by three adaptive fuzzy sliding mode controllers, each of which treats each subsystem as a single input nonlinear system. Newton-Euler mechanics is used to formulate the system's model. Here, the chattering issue is resolved and a robust control method is attained by integrating fuzzy control with sliding mode technique. Estimating a portion of control law that is equivalent to an adaptive mechanism is difficult part. In addition, the striking control was created to guarantee the system's stability. Only parameters of rules are automatically changed, though, and in order to prevent it from having a heavy computational load. Two distinct control strategies were used to demonstrate how to regulate a satellite attitude with determination by J. Chen and Y. Xu.and S Ceren [10],[12],[13],[14]. The linear quadratic regulator (LQR) with magnetic torque as an actuator was selected for attitude stabilization. Additionally, a linear regulator was used as a controller with reaction wheels as an actuator for attitude maneuvering.

In addition to introducing and formulating environmental disturbance torques using quaternion configuration, a linearized system model has been produced and the model modified for the unique BILSAT-1 properties. Analysis is done on Turkey's linear and satellite control systems. The outcomes obtained using the nonlinear control techniques outlined in reference[15] are then contrasted with the simulation findings. The sliding mode regulator performs better than the linear controller in terms of reaction time. According to the simulation results, when there is no actuator impairment occurring in the system, a linear regulator performs rather similarly to a nonlinear regulator. For satellite attitude tracking, Shan, Gao, Li You, Xue Huifeng, and Yao ShuYue [16],[17],[3] have suggested a sliding mode surface in conjunction with a conventional PD controller. The Euler axis parameter is used to guarantee the intended dynamic trajectory while taking control torque and angular velocity into account as constraints.

Finding the idea PD parameters is one of the most difficult issues, though, and suggested method is rather complex and tricky to apply in real-world engineering contexts. For the purpose of controlling satellite attitude with time-changing inertia, Jin and Rongyu [18] have presented linear parameter variable (LPV) gain-scheduling algorithms. It uses linear matrix inequalities (LMIs) as basis for its design. The attitude sensors are gyros and star sensors, and the satellite actuators are three orthogonally positioned reaction wheels. Additionally, the controller architecture accounts for possible problems like saturation and actuator failures. By modifying the gain of the necessary controller parameters when there is a quick variation of inertial gain on the satellite dynamics, the suggested controller guarantees system performance.

The performance and robustness of CubeSat attitude and position control systems based on the Linear parameter-varying controller (LPV) and Twisting second order sliding mode (T2S) controller have been compared by Capello, Elisa, Hyeongjun Park, and Francesco Cipro[19] for small satellite attitude stabilisation. Rather, a simplified model is used to analyse the performance and behaviour of the used controller for the position control problem. Additionally, the suggested method is demonstrated by taking into account the square pyramidal reaction wheel configuration. Benefits of this arrangement include minimising torque cancellation between wheels and optimising torque generation in all directions. In the meantime, it offers a redundancy in case one wheel fails.

Lastly, in addition to undershoot and overshoot on quaternion findings, the evaluation (T2S) with sign control law shows the worst chattering phenomena in angular velocity. The stabilization objective has been accomplished in spite of these obstacles. Conversely, linear parameter fluctuation produces smooth quaternion results, but it also causes some chattering in the control input for a limited period of time. A PID controller has been developed by Raja, M., et al [20] for satellite attitude determination and stabilization, and Singular Value Decomposition has been used to determine the best attitude matrix. As a result, it supplies the corresponding quaternions[21]. For attitude control and failure analysis of small satellites under plant uncertainty and actuator failure, have developed a linear robust controller, especially a H-infinite controller with LMIs formulation. Thus, linearization of the system model is required. Nevertheless, the controller parameters are manually adjusted, and the problem detection technique is not more sophisticated. Using a reaction wheel as an actuator, H. Kaplan and S. Soner [22] suggested dynamic modelling and simulation of nonlinear LEO satellites. The simulation is implemented by considering the BILSAT-1 parameters. Satellite attitude has been manipulated using quaternion parametrization with a sliding mode regulator[5]. A brief mention is made of the choice of sensors for detection and actuators for control.

The literature mentioned above highlights various ways in which a controller affects system performance and main goal is to optimize control parameters for attitude control system and deliver high-quality angle reorientation. In order to get around singularity issue, equations are also constructed using unit quaternions configuration instead of Euler (do not experience gimbal lock). Additionally, tune fuzzy sliding mode controllers with important sliding parameters are created in order to simplify the controller's ability to separately regulate three-axis attitude. In many uncertain systems, suitable controller gain levels are required to guarantee stability and robust performance. Various implications of controller on system performance are highlighted in literature mentioned above. Providing high-quality angle reorientation and control parameter optimization for attitude control system is the sole goal of this thesis. Additionally, in order to get around the singularity issue (to not experience gimbal lock), equations are generated using the unit quaternions configuration instead of Euler. In order to simplify the controller's ability to independently regulate the three-axis attitude, adjusting fuzzy sliding mode controllers and PID with important sliding parameters are created. Optimal controller gain levels are required in many uncertain systems to provide stability and reliable performance.

# Chapter 3

# Research Methodology

## 3.1 Introduction

This paper part is focused on providing a very detailed description of a research methodology that can define how research is done related to the objective of the study.

## 3.2 The Attitude Determination and Control System

ADCS is comprised of two subsystems: Attitude determination defined as the determination of orientation of a spacecraft with respect to an inertial reference or a target such as the Earth [23]. The process includes measuring all of sensors and mathematically modelling them into an inertial frame are represented by quaternions, Euler angles or rotation matrices and then detecting in body coordinates of its components. Attitude control is dedicated to providing establishing and maintaining the spacecraft's selected orientation in a space environment. Notably, it has two of its essential characteristics are attitude maneuver control and attitude stabilization. The attitude maneuver control is direct change of spacecraft's orientation from one position to another and the attitude stabilization guarantees that maintain its existing orientation with respect to an external reference. Forces needed for these adjustments in attitude control system are provided by actuators and controls.The torque necessary to change the attitude of a spacecraft must be applied via either active or passive actuators. A block diagram generally describes the action of external forces acting on the satellite and other systems that determine its attitude [18].

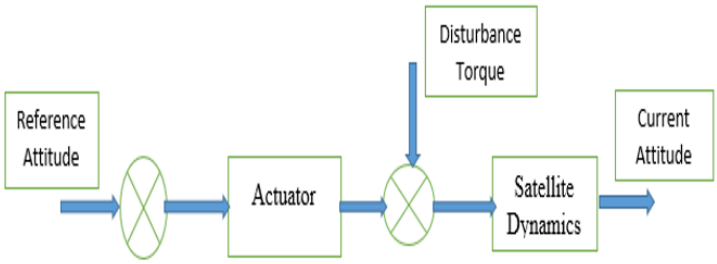


Figure 3.1: Open Loop Block Diagram of CubeSat's ADCS

## 3.3 Mathematical Modelling of CubeSat's ADCS

Modelling of an Determination and Control System (ADCS) is the design and analysis of a CubeSat. It is the platform on which to forward and analyse the behaviour of a spacecraft under varying conditions, so that engineers can make better informed decisions regarding the spacecraft architecture and operation. There are many ways to work , each characterized by its own strengths and weaknesses. Thus, the first step of system modelling consists of mathematical modelling, which describes dynamics within which the CubeSat executes its attitude motion. It typically includes the equations of motion and of dynamics describing the actuators ( thrusters, magnets, reaction wheels) used to set its orientation. This chapter briefly overview of orbital, particularly focusing on coordinate system transformation and complete satellite model equations, including kinematics and dynamics. The torques due to environmental disturbance are mentioned in the chapter, which are felt by the satellite [10],[3],[5],[24]. Logically a satellite is a rigid body, while it is acted upon external forces and moments. This is further conditioned in the form of a complete body, but quite a number of mass points are held fixed with respect to the other parts of the body. The referenced expressions have been derived from [1],[25],[26].Their classification is in accordance with the weight of each satellite as articulated below:

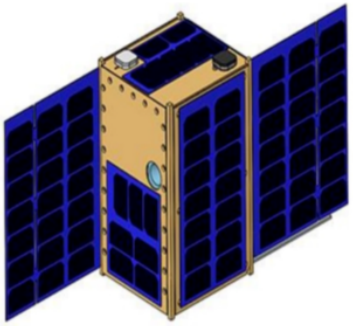

Figure 3.2: Representation of Different Types of Satellites
[25]

Table 3.1: Satellite Categories and Their Mass

| **Category** | **Mass [in Kg]** |
|---|---|
| Large satellite | ¿1000 |
| Medium satellite | 500 to 1000 |
| Mini satellite | 100 to 500 |
| Micro satellite | 10 to 100 |
| Nano satellite | 1 to 10 |
| Pico satellite | 0.1 to 1 |
| Femto satellite | less than 0.1 |

Different frames of reference denote the mathematical model, orientation of a satellite with definitions and notations. The some basic reference systems that are quite significant and make reference to positional references in satellite attitude control [27],[9],[25].

### 3.3.1 Reference of Frames

The Basic kinematics deals with the identification of the motion with respect to a few reference frames. Reference frames are essential for ADCS of spacecraft, and they are the first conditions to determine and characterize the behaviour of a spacecraft. Different coordinate reference frames could define the position and attitude of a satellite using the orientation or attitude of an LEO spacecraft. Masses in motion with reference to one another are an airplane, itself in motion relative to the earth,to the universe, and finally, the sun relative to the Milky Way galaxy. In all cases, one set of mathematical expressions used for the describe of the motion in which one reference position with respect to another moving object must be changed [26]. Attitude of a spacecraft represented in desired frame of reference as the body frame itself depending upon the mission. The coordinates' base frames used in spacecraft applications will be explored in this section[25].

### 3.3.2 Coordinate System for Earth Center Inertial (ECI)

The Earth-Centered Inertial frame (ECI) does not rotate in space, and its origin is fixed at the center of mass of Earth. The Xi-axis of ECI points towards Vernal Equinox in the northern hemisphere right hand rule determines the direction in completing the orthogonal set, and lastly, Zi-axis points toward the celestial North Pole. Thus, the Earth's equatorial plane has been chosen as the principal plane, under which any other frame shall fall under that of ECI.

Due to this reason, Newton declared that "the Earth-Centered Inertial frame of reference shall be considered an inertial frame of reference-remains fixed in space; hence, it shall not be subject to Earth's rotation and translation. Its orientation is stable with respect to solar system during that time when its origin is fixed at the center of mass of Earth. The Y-axis obeys the right-hand Cartesian coordinate transformation, and Xi-axis points towards Vernal Equinox and Zi-axis points toward North Pole." The symbol 'I' follows it[28],[25].

### 3.3.3 Coordinate System for Earth Centered Earth Fixed (ECEF)

Coordinate Systems for Earth-Centered, Earth-Fixed Frame of Reference (Earth The ECEF enables ECEF coordinates rotated by an angle of 0° from the z-axis. Earth Centered Earth Fixed, or ECEF, is thus a geodetic reference frame that is tied to the surface of the earth and depends on the region of consideration. The reference system is marked by unit vectors named xn, yn, and zn. In each location, the xn and yn axes are basically tangent to the surface of the Earth, and zn is the polarization towards the center of the Earth, perpendicular to the plane of YZ. It is due to the optical continuity between the Earth's tangent. By convention, the axis representing xn is always pointing towards the North, and the yn – axis points to the east. ECEF is a frame fixed Earth, whereby origin is at the center of mass of the planet, with the z-axis pointing towards the North Pole. The The z axis, however, does not rotate at the same speed as the rotation of the z-axis. Earth. In this case, the main difference between ECEF consists in the fact that in ECEF, there is Earth-Centered Inertial (ECI) frame has a rotational speed of its angular velocity denoted by;

$$\omega_e = 7.2921 \times 10^{-5} \text{ rad/sec},$$

which corresponds to the Earth's rotation rate. The notation "ECEF" is used to represent this frame '[25],[29],[6],[30].

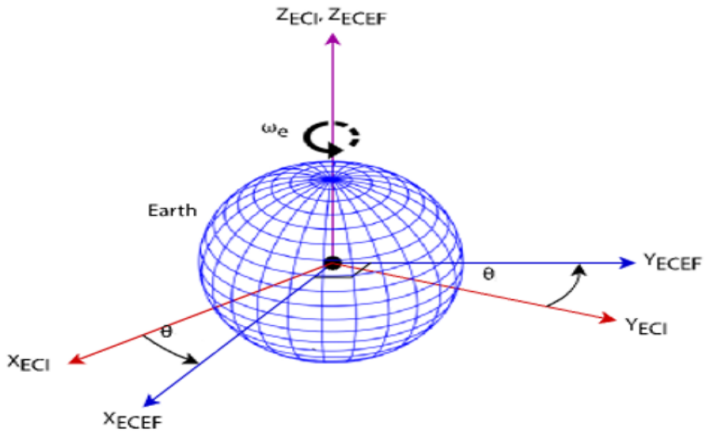


Figure 3.3: ECI and ECEF coordinate system representation [25]

### 3.3.4 Frame of Orbit

The origin in center of mass is a primitive plane from which the z-axis points along earth center in this frame. The y-axis closes the coordinate axes system per the right-hand rule, and the x-axis remains aligned with the satellite's right direction. It is given the symbol O [25].

### 3.3.5 Body Frame of the Satellite

This dynamic reference frame is firmly attached to the satellite body. Its origin is near the satellite body's center of mass. When the satellite is in attitude zero degrees in roll, pitch and yaw, the x and y axes line up with the orbit frame axes, while the z-axis points downwards through the nadir side of the satellite or to the center of the earth. It is given the symbol S. The model, however, should take into account uncertainties and nonlinearities associated with the dynamics of the CubeSat[25] .

## 3.4 The Dynamic Mode

Dynamic simulation of systems proceed through a system model of the actual system to validate all states of model. Two such important dynamic behaviours to consider in evaluating system performance of satellite designs are kinetics and attitudinal. Apart from describing how the system changes over time, differential equations offer better descriptions of the dynamics of a satellite. Mathematical methods are used to solve these differential equations and for analysing simulation dynamics. The kinematic and dynamic equations of motion provide the mathematical definition of a satellite [25].

### 3.3.1 Satellite Modelling Dynamic

A set of three differential equations describes the relationship between the force moments acting on a rotating rigid body and its angular velocity and angular acceleration. They are derived from Newton's second law, which tells us that in an inertial frame of reference, the rate of change of linear momentum of a body with respect to time is equal to the net force acting on it[25].

$$\sum F = \frac{d(m \cdot v)}{dt} = m \cdot \frac{dv}{dt} = m \cdot a \tag{3-1}$$

Where $a$ is the vector acceleration of $m$ with respect to an inertial frame, $\sum F$ is the vector sum of forces acting on mass $m$ travelling with velocity $v$, and the product $m \cdot v$ is the linear momentum.

$$r \times \sum |F| = \frac{d(m \cdot v)}{dt} = r \times m \cdot a = r \times m \cdot \frac{dv}{dt}$$

Where $r$ is the vector representing the distance between the item and the rotational point. The time derivative of the angular momentum is equal to the right-hand side of this equation [25].

$$\frac{d(rxmv)}{dt} = \left(\frac{d(r)}{dt} \times mv\right) + \left(rx \cdot m \cdot \frac{dv}{dt}\right)$$

$$\frac{d(rxmv)}{dt} = v \times mv + \left(rx \cdot m \cdot \frac{dv}{dt}\right)$$

$$\frac{d(rxmv)}{dt} = rx \cdot m \cdot \frac{dv}{dt}$$

$$rx \sum F = \frac{dH}{dt}$$

$$\sum M = \frac{dH}{dt} \tag{3-2}$$

Where $H$ represents the total angular momentum of the rigid body about its center of mass, while $M$ denotes the sum of external moments exerted in the center of mass. The total angular momentum vector $H$ of the satellite relative to an inertial fixed reference frame is determined by:

$$H = I \cdot \omega_{b/i} \tag{3-3}$$

Where $I$ is the spacecraft's moment of inertia and $(\omega_{b/i})$ is the body frame's angular velocity in relation to an inertial frame. The satellite's moment of inertia in this study is expressed as follows:

$$I = \begin{bmatrix} I_x & 0 & 0 \\ 0 & I_y & 0 \\ 0 & 0 & I_z \end{bmatrix} \tag{3-4}$$

Since the reference frame of the rigid body is stationary within the body but rotates with respect to the inertial frame, equation (3.2) becomes:

$$\left[\frac{dH}{dt}\right]_{\text{Inertia}} = \left[\frac{dH}{dt}\right]_{\text{Body}} + \omega_{b/i} \times H = M \tag{3-5}$$

Rotational equation of motion for the rigid body about its center of mass can be expressed as follows:

$$M = \frac{d(I \cdot \omega)}{dt} + \omega \times (I \cdot \omega) \tag{3-6}$$

Where $(\omega_{b/i})$

$$\begin{bmatrix} M_x \\ M_y \\ M_z \end{bmatrix} = \begin{bmatrix} I_x & 0 & 0 \\ 0 & I_y & 0 \\ 0 & 0 & I_z \end{bmatrix} \begin{bmatrix} \dot{\omega}_x \\ \dot{\omega}_y \\ \dot{\omega}_z \end{bmatrix} + \begin{bmatrix} \omega_x \\ \omega_y \\ \omega_z \end{bmatrix} \times \begin{bmatrix} I_x & 0 & 0 \\ 0 & I_y & 0 \\ 0 & 0 & I_z \end{bmatrix} \begin{bmatrix} \omega_x \\ \omega_y \\ \omega_z \end{bmatrix} \tag{3-7}$$

Computing the cross product and matrix multiplication yields:

$$\begin{bmatrix} M_x \\ M_y \\ M_z \end{bmatrix} = \begin{bmatrix} \dot{\omega}_x I_x \\ \dot{\omega}_y I_y \\ \dot{\omega}_z I_z \end{bmatrix} + \begin{bmatrix} \omega_y \omega_z I_z - \omega_y \omega_z I_y \\ \omega_x \omega_z I_x - \omega_x \omega_z I_z \\ \omega_x \omega_y I_y - \omega_x \omega_y I_x \end{bmatrix}$$

As an alternative, the roll, pitch, and yaw axes' dynamic equations can be written as follows:

$$M_x = \dot{\omega}_x I_x + (I_z - I_y)\omega_{yz} \tag{3-8a}$$

$$M_y = \dot{\omega}_y I_y + (I_x - I_z)\omega_{zx} \tag{3-8b}$$

$$M_z = \dot{\omega}_z I_z + (I_y - I_x)\omega_{xy} \tag{3-8c}$$

### 3.4.1 Satellite Model Kinematics

The study of how objects move without taking into account the mechanisms underlying that motion is known as kinematics. The orientation of a rigid body in rotational motion is described by a kinematics equation. Since there are no forces involved in the motion, it is mathematical. There are two modes of operation, one appropriate for small angles and the other for big angles, depending on the system's specifications, including pointing precision and angle value[25],[31],[32] .

### 3.4.2 Angles of Euler

In contrast to point mass systems, a rigid body is a solid object with an orientation or attitude. The Euler angles are a collection of three sequential rotations ($\theta_1$, $\theta_2$, and $\theta_3$) about designated body axes that were introduced by the mathematician and physicist Leonhard Euler. 1, 2, and 3 are the names of the axes. A revolution about the x-axis is represented by a 1-rotation, a rotation about the y-axis by a 2-rotation, and a rotation about the z-axis by a 3-rotation in the conventional Cartesian frame. This technique is applied when a small angle and good pointing precision are needed. An attitude matrix is obtained by rotating the three Euler angles roll ($\phi$), pitch ($\theta$), and yaw ($\Psi$) around intermediate coordinate axes [23],[25].

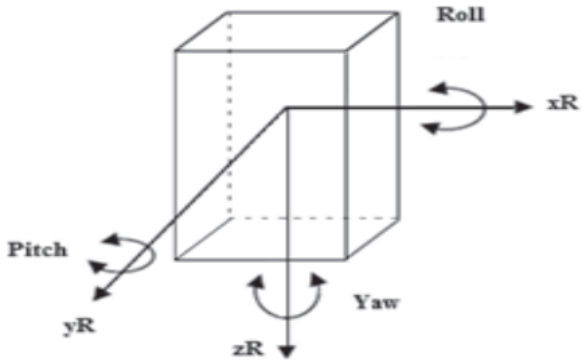


Figure 3.4: Roll, Pitch, and Yaw Angles
[25]

A total of twelve sets of body-axis rotations are conceivable. As a result, twelve sets of Euler angles are feasible. The orientation of a rigid body is described by the 3-2-1 Euler angles, which are represented by the symbols $\Psi$, $\theta$, and $\phi$. Here, the heading or yaw angle is represented by $\Psi$, the pitch angle by $\theta$, and the roll angle by $\phi$. The yaw-pitch-roll angles are another name for the set of Euler angles. The spacecraft is rolled ($\phi$) degrees about the x-axis, pitched ($\theta$) degrees about the new y-axis, and finally yawed ($\Psi$) about the new z-axis. This assumes that the orbital frame $(x_o, y_o, z_o)$ and the body frame $(x_b, y_b, z_b)$ coincide when the relationship between these two frames can be found. Any vector can be transformed from orbit frame to body frame by combining the outcomes of these rotations to create a direction cosine matrix. The full derivation of the direction cosine is given in the following [25]:

$$F_b = C_1(\phi) \cdot C_2(\theta) \cdot C_3(\Psi) F_o \tag{3–9}$$

When $F_b$ and $F_o$ stand for body and orbit frame, respectively, and the equation below:

$$\begin{bmatrix} X_b \\ Y_b \\ Z_b \end{bmatrix} = \begin{bmatrix} S_\phi S_\theta c_\Psi - c_\phi s_\Psi & C_\theta C_\Psi & C_\theta S_\Psi \\ -S_\phi S_\theta s_\Psi + c_\phi c_\Psi & s_\phi c_\theta & c_\phi S_\theta s_\Psi - S_\phi c_\Psi \\ S_\phi c_\theta & c_\phi c_\theta & \end{bmatrix} \begin{bmatrix} X_0 \\ Y_0 \\ Z_0 \end{bmatrix} \tag{3-10}$$

The angular velocity of the orbit frame $F_o$ concerning the Earth is

$$\omega_{0/i} = -\omega_0 y_0 \tag{3-11}$$

The mean orbital motion, denoted by $\omega_0$, is solved by:

$$\sqrt{\frac{\mu}{R_o^3}} \tag{3-12}$$

Where $R_o$ is the vector's radius from Earth's center to the spacecraft's center, and accordingly, the orbital motion is equivalent to the spacecraft's angular rate of motion within its orbit. The value of $\omega_0$ for a 500 km orbit altitude is $1.107 \times 10^{-3}$ rad/s.

$$\omega_{0/i} = -\omega_0 \begin{bmatrix} \sin\Psi\cos\theta \\ \sin\Psi\sin\theta\sin\phi + \cos\Psi\cos\phi \\ \sin\Psi\sin\theta\cos\phi - \cos\Psi\sin\phi \end{bmatrix} \tag{3-13}$$

With basis vectors $(X_b, Y_b, Z_b)$, the body-fixed reference frame's angular velocity is determined by

$$\omega = \omega_{b/i} = \omega_{b/0} + \omega_{0/i} \tag{3-14}$$

Additionally, the angular velocity of the body frame with respect to the orbital frame, $\omega_{b/0}$, can be expressed as follows for the sequence of $C_1(\phi) - C_2(\theta) - C_3(\Psi)$:

$$\begin{bmatrix} \omega_x \\ \omega_y \\ \omega_z \end{bmatrix} = \begin{bmatrix} 1 & 0 & -\sin\theta \\ 0 & \cos\Psi & \sin\Psi\cos\theta \\ 0 & \sin\Psi & \cos\Psi\cos\theta \end{bmatrix} \begin{bmatrix} \dot{\phi} \\ \dot{\theta} \\ \dot{\Psi} \end{bmatrix} \tag{3-15}$$

Then, by substituting (3.13) and (3.15) into (3.14), this yields

$$\begin{bmatrix} \omega_x \\ \omega_y \\ \omega_z \end{bmatrix} = \begin{bmatrix} 1 & 0 & -\sin\theta \\ 0 & \cos\Psi & \sin\Psi\cos\theta \\ 0 & \sin\Psi & \cos\Psi\cos\theta \end{bmatrix} \begin{bmatrix} \dot{\phi} \\ \dot{\theta} \\ \dot{\Psi} \end{bmatrix} - \omega_0 \begin{bmatrix} \sin\Psi\cos\theta \\ \sin\Psi\sin\theta\sin\phi + \cos\Psi\cos\phi \\ \sin\Psi\sin\theta\cos\phi - \cos\Psi\sin\phi \end{bmatrix} \tag{3-16}$$

Lastly, the following are the kinematic differential equations of a rigid body in orbit:

$$\begin{bmatrix} \dot{\phi} \\ \dot{\theta} \\ \dot{\Psi} \end{bmatrix} = \frac{1}{\cos\theta} \begin{bmatrix} \cos\theta & \sin\phi\sin\theta & \cos\phi\sin\theta \\ 0 & \cos\phi\cos\theta & -\sin\phi\cos\theta \\ 0 & \cos\phi & \cos\phi \end{bmatrix} \begin{bmatrix} \omega_x \\ \omega_y \\ \omega_z \end{bmatrix} + \frac{\omega_0}{\cos\theta} \begin{bmatrix} \sin\Psi \\ \cos\Psi\cos\theta \\ \sin\Psi\sin\theta \end{bmatrix} \tag{3-17}$$

### 3.4.3 The Quaternion

Although they are difficult to calculate, the Euler angles are simple to build and visualize. When expressing the attitude in terms of Euler angles, there is a singularity issue as well. The rigid body's orientation is described by parameters known as quaternions. The Irish mathematician Sir William Rowan Hamilton was the first to describe and use quaternions in three-dimensional mechanics in 1843. Calculations employ quaternions to get around the singularity issue. An efficient way to describe attitude coordinates is with quaternions, often known as Euler parameters . Another common set of attitude coordinates for describing huge rotations is this one [25],[33].

The quaternions rely on Euler's Rotational Theorem, which asserts that a single rotation on a fixed axis can adequately characterize the relative orientation of two coordinate systems. Three imaginary parts and one real portion make up quaternions' four dimensions. Each of these imaginary portions, denoted by the letters $i$, $j$, and $k$, has a unit value equal to the square root of $-1$; yet, they are distinct square roots of $-1$ that are all perpendicular to one another. The amount $q_0$ is a scalar part of the quaternion, while the first three components, $q_0 = (q_1, q_2, q_3)^T$, comprise a vector part. The quaternion $q = (q_1, q_2, q_3)^T$ can therefore be expressed as follows:

$$q = \begin{bmatrix} q^T \\ q_0 \end{bmatrix}$$

where the axis of rotation is described by the vector $q^T$, and the amount of rotation is described by the scalar $q_0$. The rigid body attitude is defined by the quaternion as a single rotation angle of the Euler axis. The quaternion's scalar part is associated with the rotation angle about the Euler axis, whereas its vector part shows the direction of the Euler axis.

$$q_0 = k_x \sin\left(\frac{\theta}{2}\right), q_1 \quad = k_y \sin\left(\frac{\theta}{2}\right), q_2 = k_z \sin\left(\frac{\theta}{2}\right), q_3 \quad = k_w \sin\left(\frac{\theta}{2}\right) \tag{3-18}$$

Where $(k_x, k_y, k_z)$ are the direction cosines of the Euler axis with respect to the reference frame, and $(\theta)$ is the rotation angle about the Euler axis. The differential equation for quaternion kinematics is explained by

$$\dot{q} = \frac{1}{2}\Omega \cdot q \tag{3-19}$$

Where $q = (q_1, q_2, q_3, q_0)^T$ the definition of a skew-symmetric matrix with $T$ and $\Omega$ is:

$$\Omega = \begin{bmatrix} 0 & \omega_z & -\omega_y & \omega_x \\ -\omega_z & 0 & \omega_x & \omega_y \\ \omega_y & -\omega_x & 0 & \omega_z \\ -\omega_x & -\omega_y & -\omega_z & 0 \end{bmatrix} \tag{3-20}$$

Thus equation (3-11) will be:

$$\begin{bmatrix} \dot{q_1} \\ \dot{q_2} \\ \dot{q_3} \end{bmatrix} = \frac{1}{2} \begin{bmatrix} 0 & \omega_z & -\omega_y & \omega_x \\ -\omega_z & 0 & \omega_x & \omega_y \\ \omega_y & -\omega_x & 0 & \omega_z \\ -\omega_x & -\omega_y & -\omega_z & 0 \end{bmatrix} \begin{bmatrix} q_1 \\ q_2 \\ q_3 \\ q_4 \end{bmatrix} \tag{3-21}$$

The quaternion parameters are dependent on each other, but constrained by the relationship:

$$q^T q = q_1^2 + q_2^2 + q_3^2 + q_0^2 = 1 \tag{3-22}$$

## 3.5 Dynamic Linearize Modelling

Linear equations are necessary for many applications. The satellite equation must be linearized in order to apply a linear optimum controller to the system. Euler angle functions rely on trigonometric primitives like sine and cosine [2],[34] . The linearized versions of these functions are therefore worth taking into account. Here, linearization entails substituting [25] : $\sin\delta \approx \tan\delta \approx \delta$, $\cos\delta = 1$ for small angles. Equation (3-16) then turns into:

$$\begin{bmatrix} \omega_x \\ \omega_y \\ \omega_z \end{bmatrix} = \begin{bmatrix} \dot{\phi} + \omega_o \Psi \\ \dot{\theta} - \omega_o \\ \dot{\Psi} - \omega_o \phi \end{bmatrix} \tag{3-23}$$

$$I_X \ddot{\phi} - \omega_o^2 (I_z - I_y)\phi - \omega_o (I_x + I_z - I_y)\dot{\Psi} = M_x \tag{3-24a}$$

$$I_y \ddot{\theta} = M_y \tag{3-24b}$$

$$I_z \ddot{\Psi} + \omega_o^2 (I_y - I_x)\Psi + \omega_o (I_z - I_y - I_x)\dot{\phi} = M_z \tag{3-24c}$$

Motion in the roll and yaw axes is treated as a Multi Input Multi Output (MIMO) system, while the motion in the pitch is treated as a Single Input Single Output (SISO) system. This is because the motion in pitch is independent, while the motion in roll and yaw is coupled through the orbit rate, as shown by equations (3-24 a, b, and c) [25] . It is possible to rewrite equations (3-24 a, b, and c) as follows:

$$\ddot{\phi} = \frac{1}{I_x} \left( \omega_o^2 \left( (I_z - I_y)\phi + \omega_o (I_x + I_z - I_y)\dot{\Psi} + M_x \right) \right) \tag{3-25a}$$

$$\ddot{\theta} = \frac{M_y}{I_y} \tag{3-25b}$$

$$\ddot{\Psi} = \frac{1}{I_z}\left(-\omega_o^2(I_y - I_x)\Psi - \omega_o(I_z - I_y + I_x)\dot{\phi} + M_z\right) \tag{3-25c}$$

## 3.6 Disturbance Torques Analysis

Calculate the total disturbance torque based on the worst-case scenario, where the maximum values will be considered. One orbit time, or roughly $T = 1000$ sec, is used for analysis. The spacecraft's mass is $m = 1.33$ kg, and its altitude is approximately $h \approx 400$ km [35]. These are preliminary considerations on the spacecraft's parameters before looking at mathematical representations of disturbance torques. Additionally, a number of characteristics must be taken into account, such as the maximum exposed area, drag coefficient, and maximum moment arm. When a disturbing force aligns with one of the cube's diagonals, the cross-sectional area exposed to that force is at its maximum. Then, $A_{\max} \approx 0.01732\, m^2$ is the maximum exposed area [36].

Given that the reference spacecraft is a CubeSat, it may be roughly represented as a cube, and according to , the drag coefficient of a cube is $C_d = 2.22$. For reference spacecraft, the max moment arm is defined as the distance between the spacecraft's center of mass and the centroid of the surface, or $L = 0.01$ m . There are multiple types of torque acting on the satellite body. Aerodynamics, magnetic fields, solar radiation, and gravity gradients are the four main categories of external disturbance torques. A number of variables influence the amplitude of each disturbance torque and, consequently, the dominant type of torque, including orbit altitude, mass characteristics, spacecraft geometry, and spacecraft orientation [25].

### 3.6.1 Torque from Gravity Gradient

According to Newton's Law of Universal Gravitation, gravity gradient torque is dependent on changes in the gravity field. The side of the spaceship that is closest to Earth feels the most gravitational pull, whereas the side that is further from Earth feels the lightest pull. The spacecraft rotates until it aligns along its least inertia axis due to torque produced by the variations in gravitational attraction along the spacecraft. Since gravity gradients will induce the spacecraft to rotate into a particular direction, irregularly shaped spacecraft are particularly vulnerable to gravity gradient torques. Assume that the moving satellite is located $R_o$ away from Earth's center of mass.

Gravity gradient torques caused from the lower mass element of the spacecraft are subjected to exponentially higher gravity forces than upper mass elements [37]. The unit vectors of body coordinates axis frame are $\mathbf{i}_B, \mathbf{j}_B$, and $\mathbf{k}_B$; $\rho$ is the distance

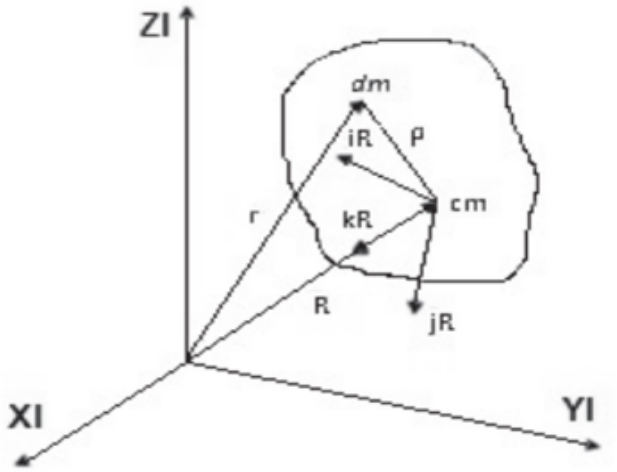


Figure 3.5: Moments of gravity on an asymmetric spacecraft [25]

between the body's cm and any mass element $dm$ in the body; and attractive gravity force is aligned along the $k_R$ axis. Using any of Euler angle transformations, determine components of the vector $\mathbf{R} = -R_o\mathbf{k}_R$ in the body axis. The labels $R_x, R_y$, and $R_z$ applied to the body axes' components of vector $\mathbf{R}$. We've

$$\begin{bmatrix} R_x \\ R_y \\ R_z \end{bmatrix} = \mathbf{A} \begin{bmatrix} 0 \\ 0 \\ -R_o \end{bmatrix} \tag{3-26}$$

It follows that

$$\begin{aligned} R_x &= R_o \sin\theta = A_{13}(-R_o) \\ R_y &= -R_o \sin\phi\cos\theta = A_{13}(-R_o) \\ R_z &= -R_o \cos\phi\cos\theta = A_{33}(-R_o) \end{aligned} \tag{3-27}$$

$\mathbf{G} = [G_x, G_y, G_z]^T$ is the definition of the gravity gradient vector. The force that gravity applies to a mass element is

$$dF = -\left[\frac{\mu\, dm}{|r|^3}\right]\mathbf{r}$$

Where $\mathbf{r} = \mathbf{R} + \rho$ is the distance from Earth's cm to mass $dm$. Since $\rho \ll R_o$, the moment about cm of body becomes.

$$D_g = \rho \times dF = -\frac{\mu\, dm}{|r|^3}\rho \times \mathbf{r} \tag{3-28}$$

Where $\rho$ is the radius vector from the body center of mass to a generic mass element $dm$. With $\rho \ll R_o$, $\frac{1}{|r|^3}$ can be approximated as

$$\frac{1}{|r|^3} \approx \frac{1}{R_o^3}\left[1 - \frac{\mathbf{R}\cdot\rho}{R_o^2}\right] \tag{3-29}$$

When Equation (3-28) and Equation (3-29) are integrated over the full body mass, the result is

$$\mathbf{G} = \frac{3\mu}{R_o^5}\int_M [\mathbf{R}\cdot\rho]\,[\rho\times\mathbf{R}]\,dm \tag{3-30}$$

After calculating scalar and vector products, it becomes

$$\begin{aligned} T_{G_x} &= \frac{3\mu}{2R_o^3}(I_z - I_y)\sin(2\phi)\cos^2(\theta) \\ T_{G_y} &= \frac{3\mu}{2R_o^3}(I_z - I_x)\sin(2\theta)\cos(\phi) \\ T_{G_z} &= \frac{3\mu}{2R_o^3}(I_x - I_y)\sin(2\theta)\sin(\phi) \end{aligned} \tag{3-31}$$

These are components of $\mathbf{G}$ that represent gravity gradient moment. The transition of attitude angles of body axis frame to those of reference axis frame yields elements of direction cosine matrix, which can also be used to describe gravity moment vector $\mathbf{G}$ in terms of Euler angles. By linearizing equations (3-31) for a body in a circular orbit and using small-angle approximations for $\dot{\theta}$ and $\dot{\phi}$, the linearized form of the gravity gradient torque can be obtained by inserting equation (3-12) into equation (3-31).

$$\begin{aligned} T_{G_x} &= 3\omega_0^2(I_z - I_y)\phi \\ T_{G_y} &= 3\omega_0^2(I_z - I_y)\theta \\ T_{G_z} &= 0 \end{aligned} \tag{3-32}$$

Where gravity gradient torque about Roll, Pitch, and Yaw axes is denoted by $T_{G_x}, T_{G_y}$, and $T_{G_z}$, respectively. Equation (3-32) can then be substituted into equation (3-25), which results in:

$$I_x\ddot{\phi} = -4\omega_0^2(I_y - I_z)\phi + \omega_0(I_x - I_y + I_z) \tag{3-33a}$$

$$I_y\ddot{\theta} = -3\omega_0^2(I_x - I_z)\theta \tag{3-33b}$$

$$I_z\ddot{\Psi} = -\omega_0^2(I_y - I_x)\Psi - \omega_0(I_x - I_y + I_z)\dot{\phi} \tag{3-33c}$$

It represents satellite linearized equations with gravity gradient torque.

### 3.6.2 Torque in Magnetic Fields

A spacecraft experiences mechanical torque when a magnetic moment created inside it interacts with the Earth's magnetic field. The field generated by the satellite's magnetic disturbances and control torques makes up the satellite's magnetic field. Since the regulated magnetic field is thought to be far larger than the magnetic disturbance, it is disregarded, and Cubesat uses three magnetic coils as its actuator. The magnetic coils' fundamental concept is predicated on how they interact with the Earth's magnetic field. As currents run through its windings, the magnetic coil creates a magnetic dipole that is proportional to the ampere-turns and the coil's enclosed area [25],[37]. The formula for the torque produced by the magnetic coils is

$$T_{bm} = m_b \times \mathbf{B}_b. \tag{3–34}$$

Where $\mathbf{B}_b = \begin{bmatrix} B_{bx} \\ B_{by} \\ B_{bz} \end{bmatrix}$ and $m_b$ is the generated magnetic moment inside the body.

$$m_b = m_{bx} + m_{by} + m_{bz} = \begin{bmatrix} N_x i_x A_x \\ N_y i_y A_y \\ N_z i_z A_z \end{bmatrix} = \begin{bmatrix} m_x \\ m_y \\ m_z \end{bmatrix}$$

Where $A_k$ is the coil's span area, $i_k$ is the coil current, and $N_k$ is the magnetic coil's number of windings. The magnetic torque can thus be easily represented as follows:

$$T_{bm} = S(m_b)\mathbf{B}_b = \begin{bmatrix} m_y B_{bz} - m_z B_{by} \\ m_z B_{bx} - m_x B_{bz} \\ m_x B_{by} - m_y B_{bx} \end{bmatrix}$$

or

$$\begin{bmatrix} T_{mx} \\ T_{my} \\ T_{mz} \end{bmatrix} = \begin{bmatrix} m_y B_\Psi - m_z B_\theta \\ m_z B_\phi - m_x B_\Psi \\ m_x B_\theta - m_y B_\phi \end{bmatrix} \tag{3-35}$$

Where $m_x, m_y$, and $m_z$ stand for magnetic moments, $B_{ij}, B_j$, and $B_i$ for the effect of the Earth's magnetic field on the Roll, Pitch, and Yaw axes, and $T_{mx}, T_{my}$, and $T_{mz}$ for the magnetic torques about the Roll, Pitch, and Yaw axes, respectively. The satellite will then be positioned in the proper attitude by the actuator effect of the magnetic torques reacting with the Earth's magnetic field. Magnetometers are used to measure the geomagnetic field.

### 3.6.3 Torque from Aerodynamics

The primary disturbance torque affecting the spacecraft at an orbit of 400 km or less is the aerodynamic forces. The spacecraft is experiencing this torque as a result of atmospheric drag, which is influenced by both the form factor of the object entering the atmosphere and the density of the atmosphere. The spacecraft's center of mass is where the aerodynamic torque operates. The existence of neutral gas molecules in the Earth's upper atmosphere causes aerodynamic torque, which alters the orbit shape and influences the spacecraft's velocity. This torque is nearly insignificant at higher altitudes because aerodynamic disturbances diminish with altitude. It is challenging to compute aerodynamic torque when the atmospheric density fluctuates with solar activity and the cross-sectional area changes quickly over time. The following equations can be used to determine the aerodynamic torque [25],[37] :

$$T_a = F(C_{pa} - C_g) \tag{3-36}$$

Where

$$F = 0.5(\rho C_d A V^2) \tag{3-37}$$

Where:

- $C_d$ is the coefficient of drag.
- $A$ is the area of cross-section ($m^2$).
- $V$ is the velocity of the spacecraft (m/s).
- $C_{pa}$ is the centre of aerodynamic pressure.
- $\rho$ is the atmospheric density ($kg/m^3$), and $C_g$ is the center of gravity.

### 3.6.4 Torque from Solar Radiation

Photons colliding with the spacecraft's surface produce the solar radiation force. On the surface of the spacecraft, incident photons can emit the most force when reflected in a specular form, the second-largest force when reflected diffusely, the smallest force contribution when absorbed, or they can pass through the surface.

In low Earth orbit, the torque caused by solar pressure is thought to be negligible enough to be ignored, making it the primary disturbance torque for geosynchronous spacecraft . Equations (3-38) and (3-39) can be used to compute the solar radiation torque [25],[37]. :

$$T_{sp} = F(C_{ps} + C_g) \tag{3-38}$$

$$F = \frac{F_s}{cA_s}(1+q)\cos(i) \tag{3–39}$$

Where:

- $F_s$ is the solar constant.
- $C$ is the speed of light.
- $A_s$ is the surface area.
- The center of solar pressure is $C_{ps}$.
- $C_g$ stands for center of gravity.
- $q$ is the reflectance factor.
- $i$ is the Sun's angle of incidence in degrees.

## 3.6 Complete Linearized Mathematical Modelling of ADCS CubeSat

Equation (3-35) is added to equation (3-33) to produce the final linearized attitude dynamic model of the satellite, which includes magnetic coil torque and gravity gradient torque expressed in body frame components [25].

$$I_x\ddot{\phi} = -4\omega_0^2(I_y - I_z)\phi + \omega_0(I_x - I_y + I_z)\dot{\Psi} + (m_yB_\Psi - m_zB_\theta) \tag{3-40a}$$

$$I_y\ddot{\theta} = -3\omega_0^2(I_x - I_z)\theta + (m_zB_\phi - m_xB_\Psi) \tag{3-40b}$$

$$I_z\ddot{\Psi} = -\omega_0^2(I_y - I_x)\Psi - \omega_0(I_x - I_y + I_z)\dot{\phi} + (m_xB_\theta - m_yB_\phi) \tag{3-40c}$$

Equations (3-40 a, b, and c) can be rewritten in the forms

$$\ddot{\phi} = \left(-\frac{4\omega_0^2(I_y - I_z)}{I_x}\right)\phi + \left(\frac{\omega_0(I_x - I_y + I_z)}{I_x}\right)\dot{\Psi} + \frac{(m_yB_\Psi - m_zB_\theta)}{I_x} \tag{3-41a}$$

$$\ddot{\theta} = \left(-\frac{3\omega_0^2(I_x - I_z)}{I_y}\right)\theta + \frac{(m_zB_\phi - m_xB_\Psi)}{I_y} \tag{3-41b}$$

$$\ddot{\Psi} = \left(-\frac{\omega_0^2(I_y - I_x)}{I_z}\right)\Psi - \frac{\omega_0(I_x - I_y + I_z)}{I_z}\dot{\phi} + \frac{(m_x B_\theta - m_y B_\phi)}{I_z} \tag{3-41c}$$

The gravity gradient (GG) torque and magnetic torque effects are included in this model; the equations are ready for use with the attitude determination and control system (ADCS).

## 3.7 Description of the model

### 3.7.1 Parameters of orbit

Determines spacecraft's location with respect to the Earth and Sun in an inertial equatorial frame. Semi-major axis 600 km, eccentricity 0.001, and right ascension are the spacecraft's orbital parameters. These have been selected to meet the requirements of sensors and other equipment while amplifying disturbance torques for the purpose of studying their role in attitude control. For instance, non-null eccentricity causes variations in the magnetic and gravitational fields and ultimately provides a problem for earth horizon sensors, which are primarily made for circular orbits [25],[37].

### 3.7.2 Reference Attitude

The reference attitude is defined such that the X-axis of the spacecraft and its scientific equipment points to the target, while the Y-axis points to the Sun in order to expose solar panels to sunlight. The body-fixed reference frame is defined as: X-axis: Points to the target (nadir for Earth observation). Y-axis: Aligned with the Sun vector (maximizing solar power generation) and Z-axis: Completes the right-handed system (often along the angular momentum vector) [25],[37]. The attitude error (quaternion deviation) is computed as

$$\text{error} = q_{\text{ref}} - q_{\text{est}}$$

Where $q_{\text{ref}}$ is the reference quaternion and $q_{\text{est}}$ is the estimated attitude.

### 3.7.3 Physical characteristics, Dynamics and Kinematics

The body reference frame is aligned with the principal axes, so the inertia tensor is diagonal with diagonal terms. The variation of mass and inertia due to propellant usage will not be considered in this assignment.

The spacecraft is assumed to be a rigid body, and its dynamics are described by the Euler equation, while attitude and kinematics are represented by means of quaternions as they provide a minimal global representation without singularities and are convenient for calculations and integration [25],[37]..

### 3.7.4 Static Earth Sensor (IFEHS)

The MAI-SES (4) is a compact and high-precision Static Earth Sensor designed for attitude determination on CubeSats, NanoSats, and small spacecraft operating in Low Earth Orbit (LEO). With a narrow field of view of 7 degrees and an angular resolution better than 0.25 degrees, it offers excellent performance for Earth-pointing applications, particularly in missions requiring nadir alignment or geodetic referencing. Within the ADCS framework, the sensor is assumed to maintain consistent Earth visibility within its fine field of view, enabling accurate attitude error estimation based on horizon detection [25],[37].. The sensor operates with a data refresh rate of 1 Hz, sufficient for low-frequency feedback control loops and stable Earth-facing orientation. The sensor measures the Earth's limb angle ($\theta_{\text{limb}}$) to compute the nadir vector in the body frame. The attitude error is derived from:

$$\text{error} = v_{\text{meas}} - A_{\text{est}}$$

Where:

- $v_{\text{meas}}$: Measured Earth vector.
- $A_{\text{est}}$: Estimated attitude matrix.
- $\eta$: Gaussian sensor noise.

### 3.7.5 Gyroscope

Sensors changes in orientation using the Sagnac effect and provides extremely precise rotational rate information, in part because of its lack of cross-axis sensitivity. Unlike the classic spinning-mass gyroscope or mechanical gyroscopes, the FOG has no moving parts and doesn't rely on inertial resistance to movement. Hence, it is an excellent alternative to a mechanical gyroscope. Their ARW is $0.01/\sqrt{h}$ at a rate of 1 kHz, and RRW is $1/h$. The CubeSat is Fiber Optic Gyroscopes (FOGs) strategically aligned along its principal axes to provide accurate rotational rate measurements. These gyroscopes operate based on the Sagnac effect, whereby light traveling in opposite directions within phase shifts proportional to the angular velocity of the sensor.

The mechanism enables highly sensitive detection of spacecraft rotation without relying on inertial resistance or mechanical motion [25],[37]. Unlike traditional spinning-mass gyroscopes or resonant mechanical gyros, the FOG features no moving parts, which enhances its robustness, reduces drift, and minimizes susceptibility to cross-axis coupling. This makes it exceptionally suitable for long-duration missions and precision attitude control tasks in Low Earth Orbit (LEO) environments. The measured angular rate ($\omega_{\text{meas}}$) includes bias and noise:

$$\omega_{\text{meas}} = \beta + \eta + \eta_b$$

Where:

- $\beta$: Slowly varying bias (estimated via Kalman filtering).
- $\eta$: White noise (ARW).
- $\eta_b$: Bias drift (RRW).

### 3.7.6 Singular Value Decomposition (SVD) in Kalman Filtering

SVD can be used to determine the orientation of a CubeSat from processing sensor measurements (magnetometers). By applying SVD to the measured vectors, derive the rotation matrix, and the configuration supports singularity-free attitude tracking and robust control stability analysis [25],[37]. SVD decomposes a matrix $A$ into three other matrices:

$$A = U\Sigma V^T$$

Where:

- $U$: An $m \times m$ orthogonal matrix whose columns are the left singular vectors of $A$.
- $\Sigma$: An $m \times n$ diagonal matrix containing the singular values of $A$.
- $V^T$: The transpose of an $n \times n$ orthogonal matrix whose columns are the right singular vectors of $A$.

SVD is a valuable mathematical tool in the design and operation of CubeSat ADCS, enhancing attitude estimation, control, and sensor fusion capabilities. Its robustness and efficiency make it a preferred choice for many aerospace applications.

# Chapter 4

# Controller Design

## 4.1 Introduction

A control system's duties include detecting, controlling, and directing the primary system's activity to generate the intended result. Automation is the process of controlling the main process with control systems or other methods to reduce the influence of process variability and environmental factors on the performance of process control. Sometimes the amount of these effects and fluctuations is enough to render linear controllers ineffective. The essential duties of controllers include maintaining process control and guaranteeing consistent performance.

## 4.2 Sliding Mode Controller (SMC)

When constructing any control system, robustness to uncertainty becomes a crucial consideration. Based on the ideas of variable structure control (VSC), sliding mode control (SMC) is a reliable and easy method for controlling both linear and nonlinear systems [6]. It has shown itself to be a promising method for managing uncertain nonlinear systems. SMC is shown using the phase-plane, which is composed of the error $e(t)$ and its derivative $\dot{e}(t)$. It is evident that the state trajectory, beginning with any initial condition, reaches the surface in a finite amount of time (reaching mode) and then moves in a sliding mode towards the target.Designing a custom surface is the first stage in the SMC design process. The plant dynamics on the sliding surface is limited to the surface equations [25],[37].For system control, various control techniques have been used. The most popular variable-structure prejudice kit for a reliable nonlinear system control technique is SMC.

Trajectories are forced to converge onto a sliding manifold in a finite amount of time through sliding mode control, which also guarantees that they remain on the manifold for all future times. The difficulties presented by model uncertainties, parameter fluctuations, and disturbance rejection are successfully addressed by this method. It is a good tool for managing complex, high-order dynamic systems that function in ambiguous and uncertain environments. Lastly, it works better in many advanced technologies' linear and nonlinear systems [6].

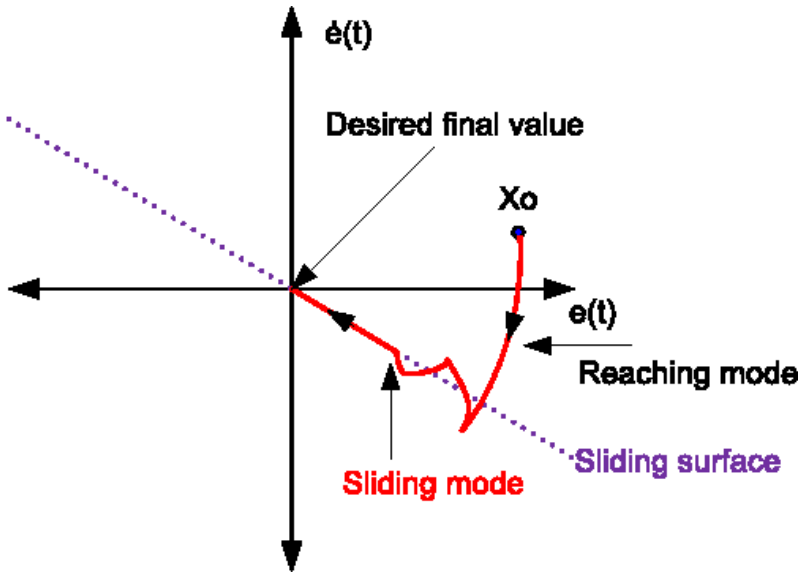


Figure 4.1: Graphical representation of SMC
[6]

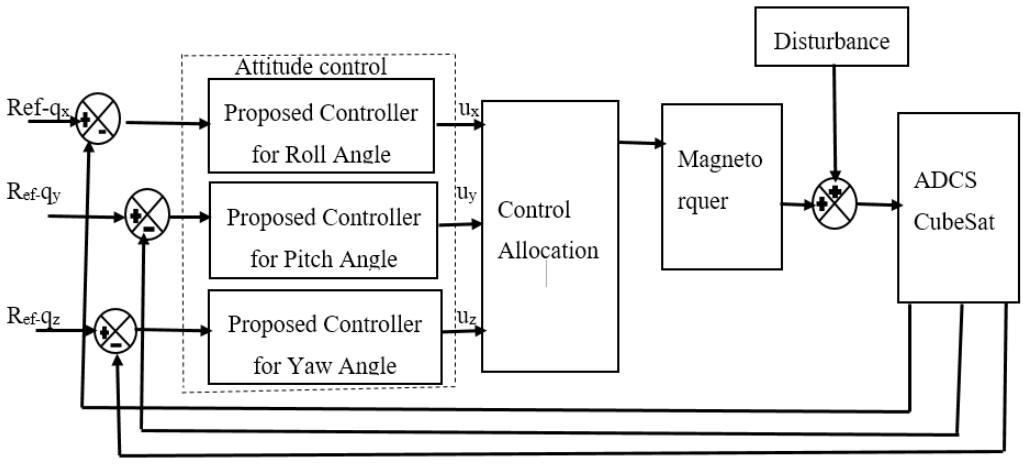


Figure 4.2: Satellite Model with Magnetorquer
[38]

### 4.2.1 State Equation of the System

Let's define quaternion error and its derivative as follows [25] :

$$qe(t) = qd(t) - qa(t) \tag{4-1}$$

$$\dot{q_e}(t) = \dot{q_d}(t) - \dot{q_a}(t) \tag{4-2}$$

$$\ddot{q_e}(t) = \ddot{q_d}(t) - \ddot{q_a}(t) \tag{4-3}$$

Where; $qd(t)\ldots$ Desired quaternion and $qa(t)\ldots$ Actual quaternion

$$\begin{bmatrix} q_{ex} \\ q_{ey} \\ q_{ez} \end{bmatrix} = \begin{bmatrix} q_{dx} - q_{ax} \\ q_{dy} - q_{ay} \\ q_{dz} - q_{az} \end{bmatrix}, \quad \begin{bmatrix} \dot{q}_{ex} \\ \dot{q}_{ey} \\ \dot{q}_{ez} \end{bmatrix} = \begin{bmatrix} \dot{q}_{dx} - \dot{q}_{ax} \\ \dot{q}_{dy} - \dot{q}_{ay} \\ \dot{q}_{dz} - \dot{q}_{az} \end{bmatrix}, \quad \begin{bmatrix} \ddot{q}_{ex} \\ \ddot{q}_{ey} \\ \ddot{q}_{ez} \end{bmatrix} = \begin{bmatrix} \ddot{q}_{dx} - \ddot{q}_{ax} \\ \ddot{q}_{dy} - \ddot{q}_{ay} \\ \ddot{q}_{dz} - \ddot{q}_{az} \end{bmatrix} \tag{4-4}$$

$$S = KPqe(t) + Ki \int_0^t Kd \frac{d}{dt} qe(t) \tag{4-5}$$

Several control techniques, including PD, PI, and PID controllers, can be used to define the sliding surface. The following is an illustration of these tactics:

$$SPD = KPe(t) + Kd \frac{d}{dt} e(t) \tag{4-6}$$

$$SPI = Kpe(t) + Ki \int_0^t e(t)dt \tag{4-7}$$

$$SPID = Kpe(t) + Ki \int_0^t e(t)dt + Kd \frac{d}{dt} e(t) \tag{4-8}$$

PID sliding surfaces have been used in SMC for satellite dynamics; the x, y, and z directions of the sliding surfaces are defined as follows, respectively:

$$\begin{aligned} S_x &= K_p q_{ex}(t) + K_i \int_0^t q_{ex}(t)dt + K_d \frac{d}{dt} q_{ex}(t) \\ S_y &= K_p q_{ey}(t) + K_i \int_0^t q_{ey}(t)dt + K_d \frac{d}{dt} q_{ey}(t) \\ S_z &= K_p q_{ez}(t) + K_i \int_0^t q_{ez}(t)dt + K_d \frac{d}{dt} q_{ez}(t) \end{aligned} \tag{4-9}$$

The control law can be computed once the sliding surface has been chosen. The system must converge to the sliding manifold according to this control law. It must remain in that position after it reaches the sliding manifold.

$$\dot{S} = K_p qe(t) + K_i qe(t) + K_d \ddot{q}_e(t) \tag{4-10}$$

$$\dot{S} = K_p[\dot{q}_d(t) - \dot{q}_a(t)] + K_i[qd(t) - qa(t)] + K_d[\ddot{q}_d(t) - \frac{1}{2}q_s\omega + \frac{1}{2}J^{-1}Hs(\omega)J\omega - \frac{1}{2}J^{-1}HU_{eq}(t)] \tag{4-11}$$

$$\omega_{bab} = \omega_{bbi} + \omega_{oc2} \tag{4-12}$$

$$J\dot{\omega} = -\omega_x(J\omega) + U + d \tag{4-13}$$

$$H = q_s I_{(3\times 3)} + \Lambda \tag{4-14}$$

$$\Lambda = \begin{bmatrix} 0 & -q_3 & q_2 \\ q_3 & 0 & -q_1 \\ -q_2 & q_1 & 0 \end{bmatrix} \tag{4-15}$$

By merging the above dynamic and kinematic equations of quaternion in chapter three, yield quaternion error derivative solved as follows;

$$\dot{q}_e(t) = \dot{q}_d(t) - \frac{1}{2}H\omega_{bab} \tag{4-16}$$

Time derivative of the above (4-16) describes as;

$$\ddot{q}_e(t) = \ddot{q}_d(t) - \frac{1}{2}(\dot{H}\omega_{bab} + H\dot{\omega}_{bab}) \tag{4-17}$$

Substituting the (4-13) and equation (4-14) in equation (4-17) yields the result:

$$\ddot{q}_e(t) = \ddot{q}_d(t) - \frac{1}{2}\dot{q}_s\omega + \frac{1}{2}J^{-1}s(\omega)J\omega - \frac{1}{2}J^{-1}HU - d \tag{4-18}$$

The control equivalent, $U_{eq}(t)$, is derived by solving the first derivative of the sliding function equate to zero, $s(t) = 0$, without considering uncertainty $d(t) = 0$, such that $e \to 0$ and $t \to \infty$.

$$\dot{S} = K_p[\dot{q}_d(t) - \dot{q}_a(t)] + K_i[qd(t) - qa(t)] + K_d\left[\ddot{q}_d(t) - \frac{1}{2}\dot{q}_s\omega + \frac{1}{2}J^{-1}Hs(\omega)J\omega - \frac{1}{2}J^{-1}HU_{eq}(t)\right] \tag{4.19}$$

$$U_{eq}(t) = 2JH^{-1}\ddot{q}_d(t) - JH^{-1}\dot{q}_s\omega + s(\omega)J\omega + \frac{2K_p}{K_d}JH^{-1}\dot{q}_e(t) + \frac{2K_i}{K_d}JH^{-1}q_e(t) \tag{4.20}$$

Total Control law is the sum of both the equivalent controller and the switching (discontinuous) controller.

$$U_{smc}(t) = U_{eq}(t) + U_{s\omega}(t) \tag{4.21}$$

$$U_{eq}(t) = \begin{bmatrix} U_{1eq}(t) \\ U_{2eq}(t) \\ U_{eq}(t) \end{bmatrix}, \quad U_{s\omega}(t) = \begin{bmatrix} U_{1s\omega}(t) \\ U_{2s\omega}(t) \\ U_{3s\omega}(t) \end{bmatrix} \tag{4.22}$$

When, the $U_{s\omega}(t)$ represents switching control that is involved when $s(e,t) = 0$, corresponds to the reaching phase, and $U_{eq}(t)$ the equivalent control corresponds to the sliding phase when $s(e,t) = 0$.

### 4.2.2 Stability Analysis

A gravity gradient stabilized system's stability and aiming ability are typically restricted. In most cases, gravity gradient alone is an inadequate method of control. It takes a long time to reach the ultimate pointing state because it is passive, and it also has weak yaw control. Magnetic coils are added to improve attitude control because the satellite cannot decrease from minor disturbances without an active controller. Therefore, in terms of both cost and performance, the gravity gradient controller can be categorized as an inexpensive and straightforward controller [25],[37].

Compared to moments of inertia about the other two axes ($I_x$ or $I_y$), $I_z$ must be substantially smaller. Usually, an explosion with a tip mass is extended to do this. When a spacecraft has explosion deployment and symmetric axes ($I_x = I_y$), the spin rate about the Yaw axis has a significant impact on roll bias. Therefore, raising the moment of inertia ratio ($I$) and decreasing the spin rate about the Yaw axis can enhance the aiming accuracy on the Roll axis. High precision cannot be attained when a nanosatellite's attitude is controlled solely by magnetic actuators due to controllability issues caused by magnetic torques being restricted on a plane perpendicular to the local magnetic field. Even though extra effort is made to minimize the disturbance torques, they nevertheless produce a significant depointing angle. Only one magneto-torquer coil can be turned on at a time due to the onboard power limitation [6]. Given the local geomagnetic field vector, a control algorithm needs to be adjusted to enable the selection of the coil that will produce the best outcomes. The Lyapunov candidate function is chosen to analyze the system's stability and is described as follows:

$$V(t) = \frac{1}{2} s^T s > 0 \tag{4-23}$$

A sufficient condition to ensure that, on both sides of $s(e,t) = 0$, the system state trajectory points in the direction of the switching surface. If and only if the Lyapunov function's derivative is negative, the system described in equation (4-23) is stable.

$$\dot{V} = s^T \dot{s} < 0 \tag{4-24}$$

Substituting the derivative of a sliding function in (4.24) above yields the reaching control signal $U_{sw}(t)$.

$$\dot{V} = s^T \left[ K_p \dot{q_e}(t) + K_i q_e(t) + K_d \left[ \dot{q}_d(t) - \frac{1}{2} \dot{q}_s \omega + \frac{1}{2} J^{-1} H s(\omega) J \omega - \frac{1}{2} J^{-1} H [U_{eq}(t) + U_{s\omega}(t)] d(t) \right] \right] < 0 \tag{4.25}$$

By rearranging the above (4-25), it becomes as follows;

$$s^T \left[ K_p \dot{q_e}(t) + K_i q_e(t) + K_d \dot{q_d}(t) - \frac{1}{2} K_d \dot{q_s} \omega + \frac{1}{2} K_d J^{-1} H s(\omega) J \omega \right] - s^T K_d \left[ -\frac{1}{2} J^{-1} H \left[ 2JH^{-1} \ddot{q_d}(t) \right] d(t) - \right. \tag{4.26}$$

$$s^T \left[ K_p \dot{q_e}(t) + K_i q_e(t) + K_d \dot{q_d}(t) - \frac{1}{2} K_d \dot{q_s} \omega + \frac{1}{2} K_d J^{-1} H s(\omega) J \omega \right] - s^T K_d \left[ \dot{q_d}(t) - \frac{1}{2} K_d \dot{q_s} \omega + \frac{1}{2} K_d J^{-1} H \right. \tag{4.27}$$

Cancel out all the same terms and ensure that the above (4-27) is less than zero, $ss\dot{s}$, Reaching control law could be selected as:

$$s^T \left[ -U_{sw}(t) + d(t) \right] < 0 \tag{4.28}$$

$$K \geq |d_{max}| \tag{4.29}$$

Reaching Law Approach: based on achieving phase system drives to the stable manifold from any initial point and it specifies the switching function dynamics. The constant rate, constant plus proportional, and power rate reaching law frameworks are the most often used in the field of reaching law. The chattering phenomenon within the overall control system will be handled by the discontinuous controller of the sign function.

It could potentially harm the mechanical system. Numerous strategies have been put up to address this problem. Similar to applying a fuzzy control method in a suitable reaching legislation. The following is the standard $U_{sw}(t)$ reaching control signal [25],[37]:

$$U_{sw}(t) = K \text{Sign}(s(t)) \tag{4.30}$$

Where, Sign(s) is a sign function, defined as:

$$\text{Sign}(s) = \begin{cases} 1, & \text{if } s > 0 \\ -1, & \text{if } s < 0 \end{cases} \tag{4.31}$$

Lastly, control signal, $U_{smc}(t)$, is reached by merging the two equations, the continuous control function $U_{eq}(t)$, and the discontinuous control function $U_{sw}(t)$, of SMC, resulting in:

$$U_{smc}(t) = 2JH^{-1}\ddot{q_d}(t) - JH^{-1}\dot{q_s}\omega + s(\omega)J\omega + \frac{2K_p}{K_d} JH^{-1}\dot{q_e}(t) + \frac{2K_p}{K_d} JH^{-1} q_e(t) - \text{Sign}[s(t)] \tag{4.32}$$

Theoretically, fuzzy logic by itself cannot ensure the stability of FSMC. To ensure boundedness and convergence, fuzzy approximations must be taken into account by expanding Lyapunov-based analysis. Formal proof cannot be replaced by simulation results, but they can be used as supporting evidence. Therefore, to show robustness and chattering suppression, a rigorous FSMC design uses simulation validation in conjunction with Lyapunov stability analysis for fuzzy systems [25],[20]..

## 4.3 Fuzzy Sliding Mode Controller Design

Fuzzy Logic is an artificial intelligence-based control method that encodes rule-based knowledge in the form of logical rules or represents expert knowledge using fuzzy rule sets and linguistic variables. L.A. Zadeh first proposed the idea of fuzzy sets in 1965. A modification to solve chattering phenomena and improve control robustness is offered by combining sliding mode control with fuzzy set theory. The goal of this thesis is to use a fuzzy logic controller in place of conventional discontinuous techniques, smoothing control operation with single-input single-output (SISO) variables. The suggested approach presents a Fuzzy Sliding Mode Controller (FSMC), which efficiently manages a nonlinear satellite model by fusing the smoothness of Fuzzy Logic Control (FLC) with the robustness of Sliding Mode Control (SMC) [39].

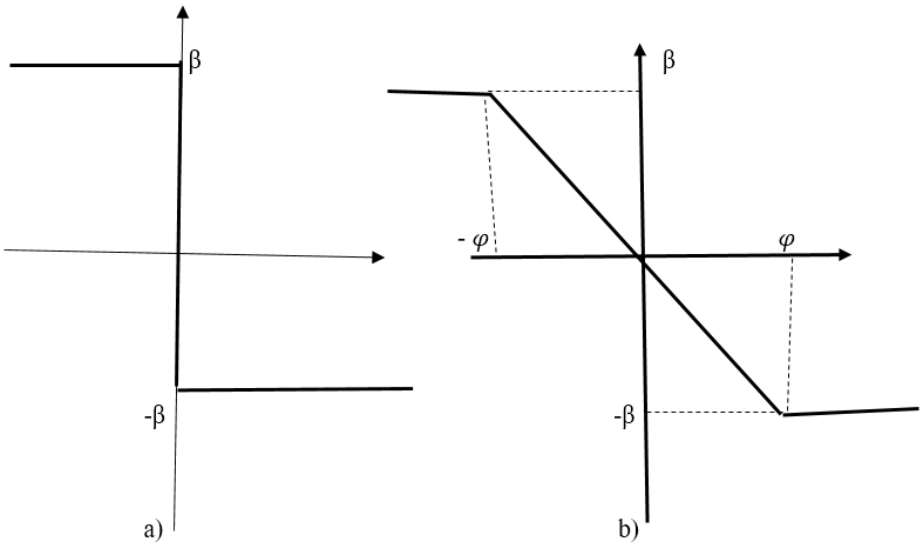


Figure 4.3: Switching function of sliding mode (a) and fuzzy sliding mode (b) [6]

The FSMC output is changed to:

$$U(t) = U_{eq}(t) + K_{sw}(t)U_{fuzzy}(t) \tag{4.33}$$

$$= U_{eq}(t) + K_{sw}(t)\text{FSMC}(s(t)) \tag{4.34}$$

When $K_{sw}(t)$ is the switching gain for fuzzy logic control and $U_{fuzzy}(t)$ is the output of fuzzy logic control. The three main stages of fuzzy logic controllers are as follows: rule evaluation, defuzzification, and fuzzification. A fuzzy logic controller's design makes a number of implicit assumptions. These assumptions are outlined as follows: First, defining the input and control variables to determine which states of the process are observed and which control actions are to be considered; second, establishing membership functions, which describe how observations of the process are expressed as fuzzy sets; third, designing the rule base, which determines which rules apply to specific states; and finally, implementing the computation algorithms that perform fuzzy computations, which typically result in fuzzy outputs [25],[37]. Design of above controllers involves selecting gains uses in the error, change-in-error, and output controllers. Each of the three axes roll, pitch, and yaw has its own fuzzy logic controller, and the design entails choosing gains that are employed in output, error, and change-in-error controllers.Figure 4-4 shows a fuzzy control system in its entirety. The interfaces for fuzzification and defuzzification provide standard options. The designer frequently chooses an inference mechanism that can be used in a variety of procedures. Therefore, the rule base is the main focus when building the fuzzy controller. This rule base is designed to simulate a human expert "in-the-loop," integrating insights from seasoned professionals who have thoroughly researched the most effective process control techniques. When such a human expert is not available, the control engineer will merely research the dynamics of the plant (perhaps with the aid of modeling and simulation) and formulate a logical set of control rules [25],[37]. For each of the three angles Roll, Pitch, and Yaw three MISO fuzzy controllers are used.

Fuzzy controller inputs include error, change of error, output, and control action. It is evident that the fuzzy logic controller offers improved stability, tighter control, and superior performance in both steady state and transient state responses, and it is sufficiently robust to any abrupt change in satellite parameters. Roll and yaw angular velocities' initial transients begin with non-zero values and swiftly drop to zero. Before settling to zero, the pitch angular velocity has a rapid transient after beginning at a much higher value. All three angular velocities attain and hold a steady-state value of zero after around one second. This suggests that the system has been successfully put into a state of rest by the Fuzzy Logic Controller (FLC). The first transients show how the FLC can react to early disruptions and start remedial measures. The quick settling to zero suggests that the FLC offers efficient control authority and dampening. When there are no oscillations in the steady state, the controller is likely well-tuned and does not overshoot. Based on the current angular velocities and their rates of change, the FLC likely applies fuzzy logic principles to choose the proper control inputs.

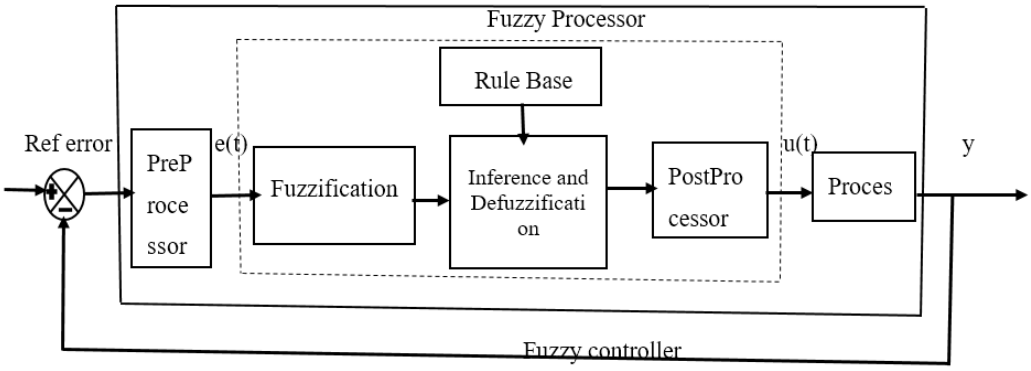


Figure 4.4: Block diagram of complete fuzzy controller
[38]

### 4.3.1 The Fuzzification Process

The process of transforming input variable values into fuzzy set membership values is known as "fuzzification." Physical input signals are modified in order to conform to the fuzzy control rule basis. Seven triangle membership functions are used in this study to fuzzify the sliding surface, represented as $s(e,t)$. Finding the extent to which input variables correspond to their respective linguistic phrases is known as fuzzification. For every linguistic word linked to the pertinent linguistic variable, the true degree of membership for each input variable is determined. Acquiring precise input values, translating them into equivalent discourse universes, and then turning the mapped data into fuzzy singletons or suitable language terms are all steps in the fuzzification process.

### 4.3.2 Rule Estimation (Knowledge Base)

To guarantee fulfillment of existence conditions, the control system's design should have included control rules that direct the state's trajectory as it bends into and slides across the sliding surface on the phase plane. To evaluate the fuzzy rules, the Mamdani fuzzy inference approach has been proposed. The sliding surface is the only input in the system, and the suggested fuzzy logic controller has a single output ($U_f(t)$). According to the rule base, fuzzy inference acts as a mechanism for mapping membership values from input to output. As a result, both the input and output have fuzzy sets or linguistic variables defined [37].

| $S(e,t)$ | NB | NM | NS | Z | PS | PM | PB |
|---|---|---|---|---|---|---|---|
| $U_{fuzzy}$ | NB | NM | NS | Z | PS | PM | PB |

Table 4.1: Fuzzy rule base

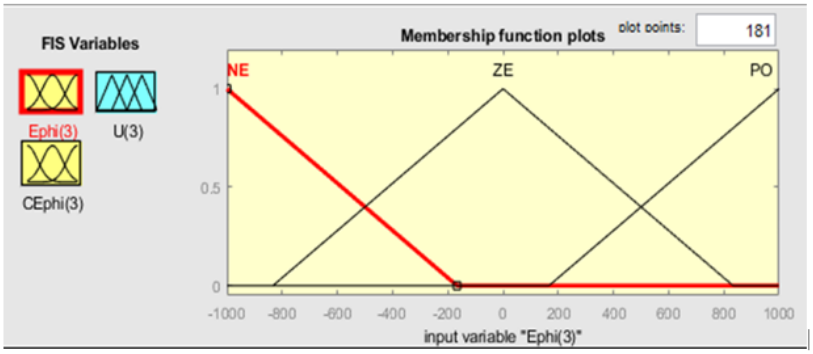


Figure 4.5: Membership functions for the input $Eh_{phi}$ of FSMC

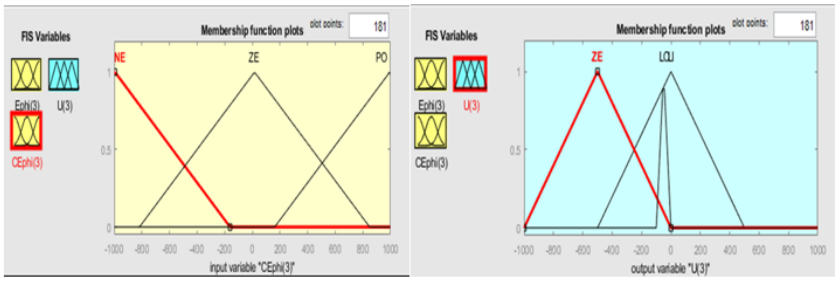


Figure 4.6: Membership functions for the input $CE_{phi}$ (Change of Error) of FSMC

### 4.3.3 Defuzzification

The outcome of the inference process must be transformed into precise numerical values since a control element is unable to process the fuzzy data directly. In order to get a single, distinct value for each output, defuzzification entails weighing and combining many fuzzy sets that come from the fuzzy inference process. Evaluations of fuzzy rules are carried out during the defuzzification process, which uses a decision-making algorithm to choose the best crisp value from a fuzzy set to translate fuzzy inference findings into a crisp output that represents the classification results for the input data [25]. As seen in Figure below, the Centre of Gravity (COG) algorithm is chosen as the defuzzification technique to convert into human understandable strings and then control the surface of $U_{fuzzy}(t)$. This can be written as follows:

$$\text{Crisp control signal} = \frac{\text{The Sum of the first Moment of Area}}{\text{Sum of Areas}} \tag{4.35}$$

$$U_{fuzzy}(t) = \frac{\int \mu(u) u \, du}{\int \mu(u) \, du} \tag{4.36}$$

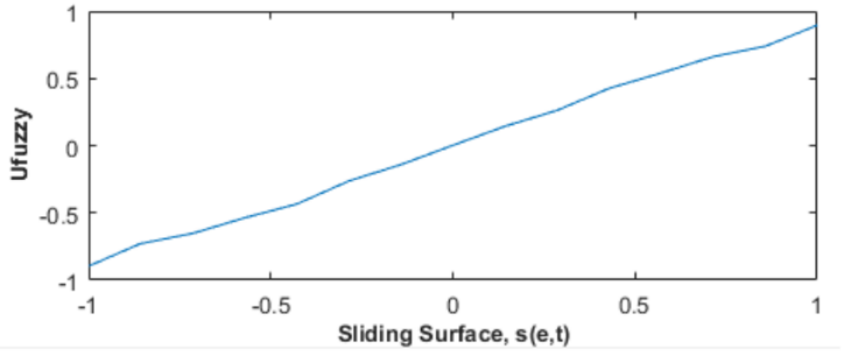


Figure 4.7: Control signal surface of FSMC

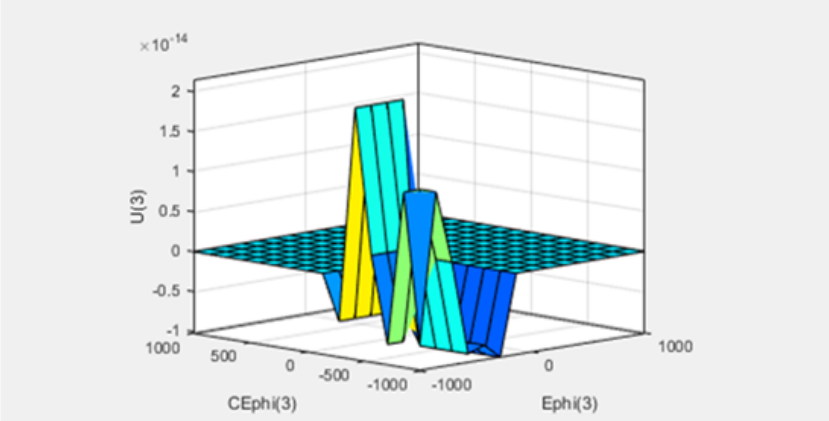


Figure 4.8: The Fuzzy Inference of System Surface

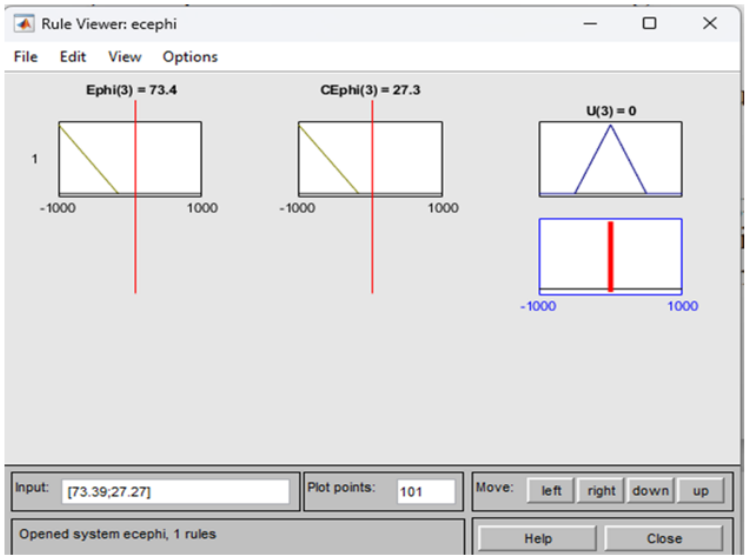


Figure 4.9: The Output of surface Rule Viewer

## 4.4 FSMC Gain Tuning

Finding the best solution to a particular issue is the optimization process. However, the most challenging parts of creating a controller for real-time applications are figuring out the ideal gain values for the suggested controller. These controller values have a significant impact on the controller's performance and optimality. Manual tuning (trial and error) is a common method that does not present design challenges, but the outcomes are not very ideal. In order to determine the ideal values for the suggested three FSMC controller gains for satellite attitude control of roll, pitch, and yaw.

The three PID sliding surface gains and switching coefficient gains for each sliding surface are listed respectively as: $[k_p(1), k_i(1), k_d(1), k_p(2), k_i(2), k_d(2), k_p(3), k_i(3), k_d(3)]$ and $[k_s(1), k_s(2), k_s(3)]$, which are tuned using PSO.

## 4.5 Particle Swarm Optimization

Bounded FSMC is known for its robustness in handling disturbances and uncertainties, making it a valuable choice for a wide array of practical control applications. However, setting the controller gains correctly is crucial to obtaining the best performance in FSMC. Traditional tuning techniques, like trial and error or manual adjustment, can be laborious, ineffective, and may not follow a methodical process. To solve this issue and ensure that FSMC operates at its best, sophisticated optimization techniques are applied. PSO is one such technique that optimizes the controller gains for FSMC. Particles are randomly selected and their movement is influenced by factors such as inertia, personal best, and global best position [25]. Each particle possesses its current objective value, position, velocity, personal best value (representing the best objective value encountered by the particle), and personal best position (the position where the personal best value was found). Besides that, PSO maintains the global best value which signifies the best objective value experienced by any particle along with the global best position representing the location where the global best value was found.

### 4.5.1 Using MATLAB-Simulink for PSO-Based Control Gain Tuning

Step 1 covers the initialization part. Create or import a Simulink model for a control system. Then add the gains or parameters that require changes during the process. Step 2 handles the algorithm setup. Using MATLAB to implement the PSO algorithm in a practical way. Parameterize it with specific settings like these. First, specify the lower and upper bounds for all the gains or parameters to adjust. Next, calculate how many particles will be in the swarm. Then declare the total number of iterations that the PSO algorithm should run. Finally, select the Integral of Time-weighted Absolute Error, or ITAE, to serve as the fitness function. Step 3: A MATLAB fitness function is used to evaluate the ITAE by simulating a Simulink model with given control parameters. The error signal is calculated by the model, and sum $\left(\int te(t)\,dt\right)$ over the time vector in the most primitive way. This function helps optimize the controller based on approaches of the Algorithm.

Step 4: To link MATLAB and Simulink for PSO optimized control systems, execute the sim command in MATLAB to ascend Simulink objects simulation with parameters; $(K_p, K_i, K_d)$ signature to the base workspace through assigning. A fitness function is MATLAB which simulates the process and calculates a performance metric such as ITAE or ISE from the output response. The Simulink model should be set up to use workspace variables and provide output signals for cost computation. This integration allows automated tuning of controllers for improved system performance. The fifth step is the PSO process loop, where the fitness evaluation of all particles' positions during each iteration will be determined by means of the PSO simulation of the system in Simulink. The sixth step involves updating the particle positions in the swarm based upon the PSO algorithm's update equations and the fit values for each particle. In addition, it is necessary to update the parameters/gains of both FLC and SMC as well as Adaptive Control.

The PSO algorithm allows for multiple iterations of optimization through repeated adjustments of all controller gains until the Integral of Time-weighted Absolute Error (ITAE) value has been minimized by means of simulation of all possible system responses. Each particle in the swarm can be considered a potential solution, with each subsequent step of the PSO algorithm based upon previous best performances. The fitness function enables all particles to be directed toward the optimum controller gain values, with this cycle continuing until a defined convergence is achieved or the maximum number of iterations has been completed.At the end of the PSO optimization process, the optimal gains set obtained from the whole swarm will be those values associated with the global best solution, producing optimal system performance based upon the definition of the fitness function. The optimal gains will then be applied to the controller to improve all operations of the system. Once all optimal gains have been obtained, those values must be re-entered into the Simulink control system model to be used in the controller.

### 4.5.2 Fitness Function

Standard performance indices (fitness or cost functions), which are well accepted by most people, can identify the optimal parameter values for controllers that produce acceptable responses from the systems being controlled [6]. There are four types of commonly used indices: IAE, ISE, ITSE, and ITAE. The thesis focuses on ITAE as the cost function because it has less overshoot, fewer oscillations with better damping, and more response to small changes in the controller parameters than the other types of cost functions. The equations for the performance criteria are given below:

$$ISE = \int_0^\infty e^2(t)\,dt \tag{4.37}$$

$$ITSE = \int_0^\infty te^2(t)\,dt \tag{4.38}$$

$$IAE = \int_0^\infty |e(t)|\,dt \tag{4.39}$$

$$ITAE = \int_0^\infty t|e(t)|\,dt \tag{4.40}$$

# Chapter 5

# Simulation Results and Discussion

## 5.1 Introduction

This section focuses on simulation and presentation of results for the attitude control problem of a rigid body spacecraft system. The simulation result indicates the effectiveness of the proposed controller based on satellite attitude maneuver. In the beginning, the linearized dynamic equation of motion with small and input torque to the system for each axis (Roll, Pitch, and Yaw) is considered. By focusing on accuracy in initial conditions, dynamics, smoothing, and interpretation, it is ensured that the CubeSat's orientation is precisely controlled. This is essential for achieving the mission objectives and maintaining stable operations in space.The adjusted parameters and longer simulation time may provide a more comprehensive evaluation of the ADCS accuracy for a CubeSat. The increased simulation duration and different initial conditions can offer insights into the long-term stability and performance of the attitude determination and control system. However, the specific criteria for accuracy assessment would depend on the mission requirements and objectives of the CubeSat. With higher angular velocities and a longer simulation span, it provides a more rigorous test of the CubeSat's ADCS, representing more realistic operational scenarios. The use of a higher number of integration steps requires careful normalization to maintain accuracy over extended periods. The linearized dynamic equation of motion with torque, parameters, initial values, and modification values of the satellite are presented in Tables . The results (attitude angles) are plotted versus orbit to indicate the number of orbits the satellite passes, and the simulations utilized parameter settings of the ADCS satellite which are detailed below [25].

Table 5.1: ADCS CubeSat parameters

[25]

| **Parameter** | **Value** |
|---|---|
| Weight | 1.33 kg |
| Size | $10 \times 10 \times 10$ cm |
| Moments of inertia | $I_x = 0.1043$, $I_y = 0.1020$, $I_z = 0.0031\,(\mathrm{kg} \cdot \mathrm{m}^2)$ |
| Boom length | 1.5 m |
| Maximum magnetic moment | 0.1 A |
| Control period | 60 Minutes |
| Orbit | 600 km |
| `Surf_nominals` | $[-0.1, 0.5]$ |
| `Surf_reflectivity` | $[0.1, 0.3, 0.5]$ |
| `Esun` | 670 |
| Earth | 1 |
| Dgh | 1.3 |
| Tmax | 0.1 |
| `TEHS_noise` | 0.01 |
| `Gyro_noise` | 0.01 |
| `Tsc` | $[0.0337, 0.1037, 0.0383]$ |

Table 5.2: Parameters with Initial and Modification Values

| **Parameter** | **Initial Value** | **Modification Value** |
|---|---|---|
| Angular Velocity | $[0\,0\,0]^T$ rad/s | $[0.0873\ -0.0873\,0.1745]^T$ rad/s |
| Euler Angles | $[0\,0\,0]^T$ rad | [0.4360 0.1614 1.134] radian |
| Quaternion | $[1\,0\,0\,0]^T$ | $[0.3288\ -0.3288\,0.3288\,0.822]^T$ |
| M-Disturbance | $[0.01\,0.05\,0.01]^T$ | [0.00005 0.00025 0.0005] J |
| Magn_noise | 0.005 | 50 |

Table 5.3: Parameters for Proposed Controller

[25]

| **Controller Type** | **Proportional Gain $K_p$** | **Derivative Gain $K_d$** | **Integral Gain $K_i$** |
|---|---|---|---|
| PID controller for Roll | 0.00021768 | $3.68030751 \times 10^{-6}$ | 0.1168967 |
| PID controller for Pitch | 1 | 1 | —— |
| PID controller for Yaw | 0.00687887 | $5.40484652 \times 10^{-5}$ | 0.07943 |

## 5.2 Simulation Results of Model Verification

Figure 5.1 shows the modified attitude control system for the CubeSat to optimize its performance controller. The roll, pitch, and yaw errors converge quickly, remaining small throughout the simulation. The transient response for all axes settles near zero around 20 to 30 seconds, with minimal overshoot.

From 30 to 80 seconds, the steady-state behavior keeps roll and pitch effectively at zero, while yaw holds near zero with only minor drift and for figure 5.2 the stabilized quaternion after modifications made to suppress oscillations in the initial dynamics. It indicates that the components converge to a steady value: $q_1$ stabilizes near 0.5, suggesting dominant orientation along the x-axis, while $q_2$ settles at -0.5, reflecting a balanced contribution from the y-axis. Components $q_3$ and $q_0$ remain near zero, confirming minimal rotation about the scalar and z-axis components.

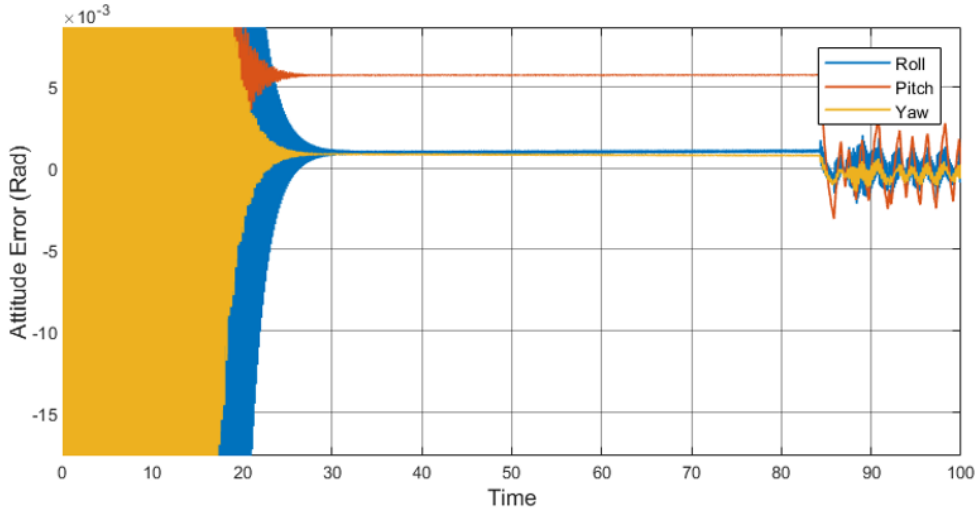


Figure 5.1: Attitude Error of Dynamics System after Modification of ADCS CubeSat

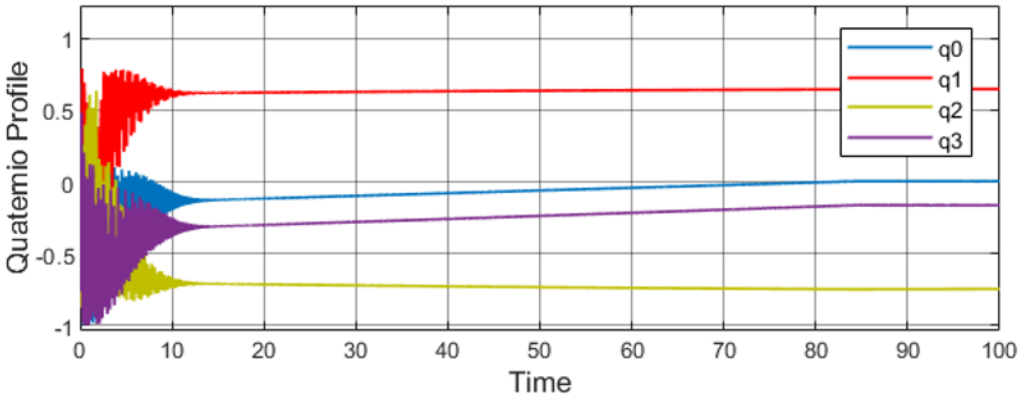


Figure 5.2: Quaternion of Attitude Control System after Modification

Figure 5.3 analyzes quaternion dynamics and SVD profiles over time. It reflects the stability and transformation characteristics of the CubeSat attitude control system. Each component stabilizes after the initial transients, indicating successful attitude convergence and Figure 5.4 shows the CubeSat body frame data from IFEHS sensors during the initial dynamics, indicating oscillatory behaviour resulting from attitude corrections and transient control responses. The damping for $w_y$ and $w_z$ demonstrates high-frequency oscillations that gradually attenuate over time, highlighting effective damping and overall stabilization in the system. Additionally, $w_x$ trends slightly downward, exhibiting some minor residual motion on the x-axis. After approximately 80 seconds, all components converge toward steady-state values.

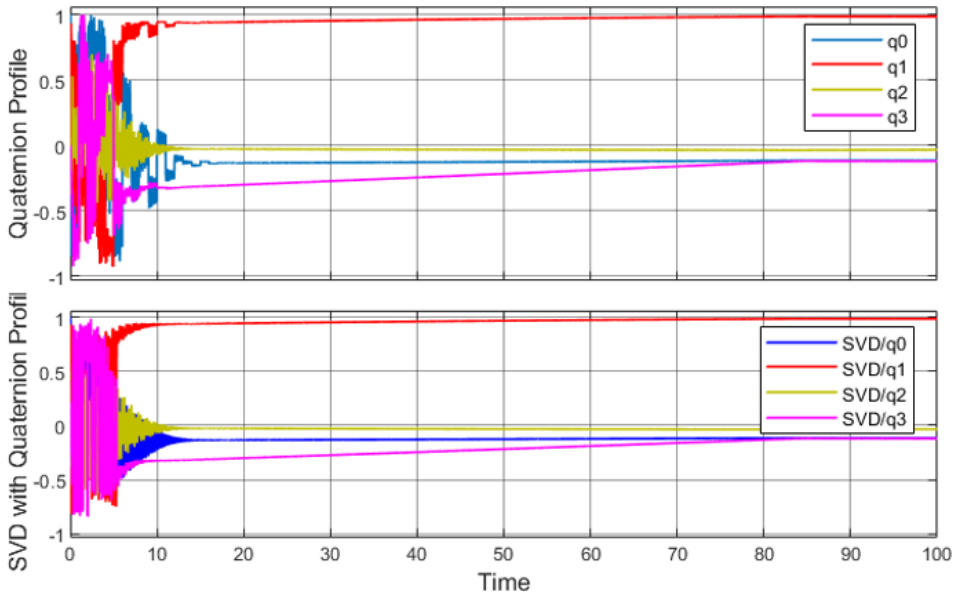


Figure 5.3: Quaternion Kinematics and Singular Value Decomposition (SVD)

Figure 5.5 depicts the initial dynamics with transient oscillations linked to attitude correction maneuvers and control activation. The damping behaviour of $w_z$ features a noticeable negative spike right at the start, indicating strong corrective torque in the early phase. Moderate oscillations appear for $w_x$ and $w_y$, gradually decaying as the system settles. Stabilization occurs between 60 and 80 seconds for most cases, with all components converging toward near-zero values and the figure 5.6 illustrates the filtered gyroscope angular velocity components ($w_x$, $w_y$, and $w_z$) in the body frame of the satellite. Initially, all components exhibit significant oscillations, which aligns with dynamic motion possibly caused by initial perturbations. Over time, the amplitudes start high but decay, demonstrating the effects of damping of attitude control algorithms that work to stabilize the system.

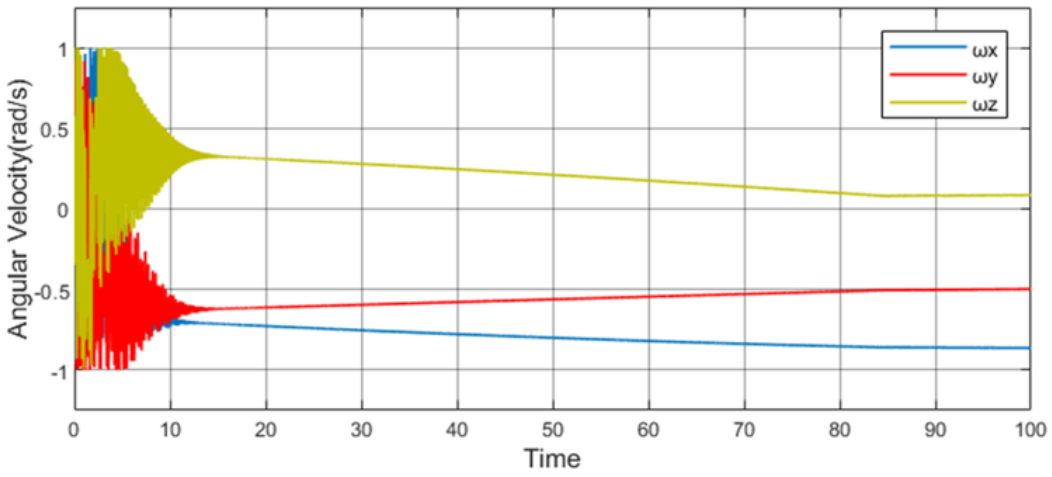


Figure 5.4: Angular Velocity of CubeSat ADCS in Body Frame ((IFEHS)

Figure 5.7 illustrates the angular acceleration response in the body frame during the initial transients from 0 to 20 seconds. It shows variations of active attitude corrections responses from control inputs and after 20 seconds, the angular accelerations converge toward zero levels, with minor residual fluctuations persisting across all axes.

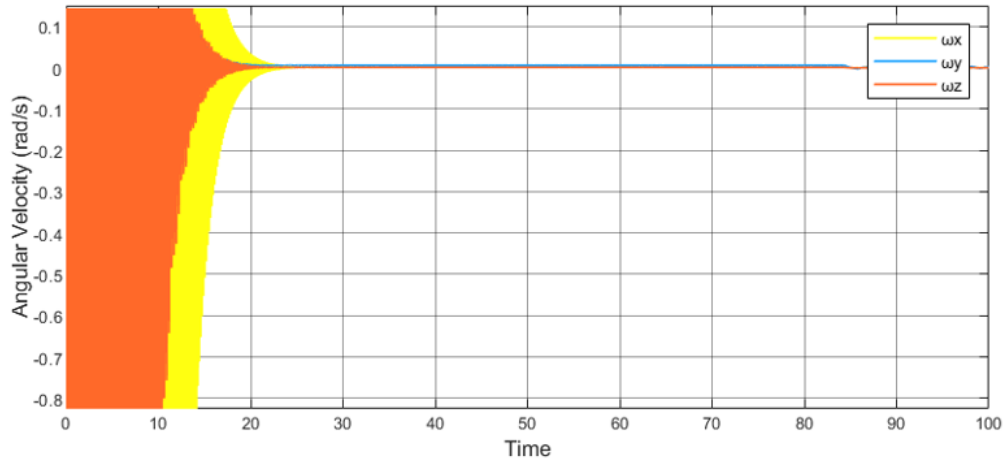


Figure 5.5: ADCS CubeSat Angular Velocity Response in Body Frame (gyroscope)

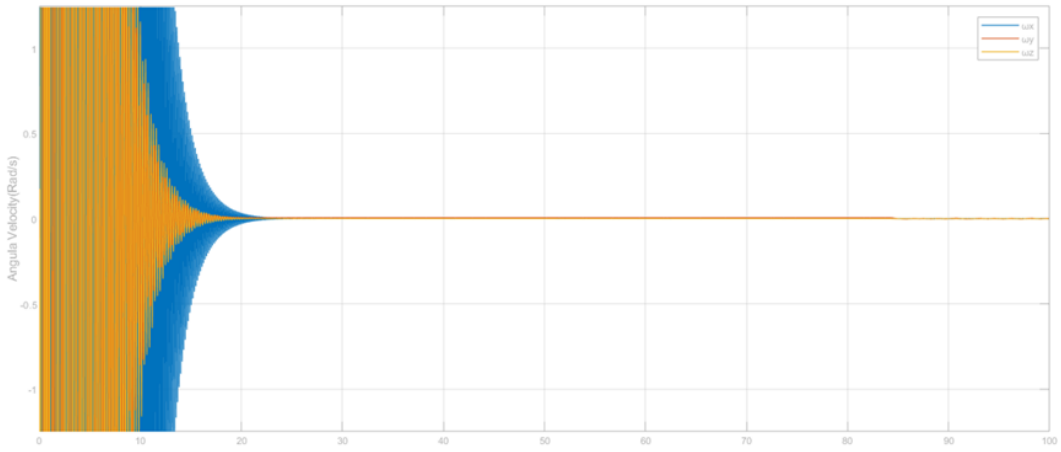

Figure 5.6: Filtered Gyroscope Angular Velocity Response in Body Frame

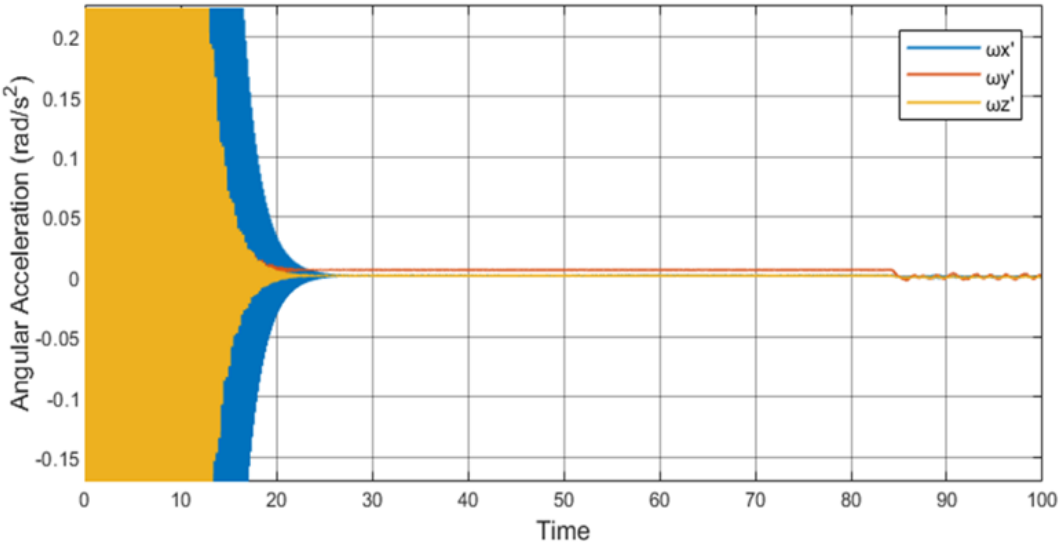


Figure 5.7: Gyroscope Angular Acceleration Response in Body Frame

Figure 5.8 illustrates that the gravity gradient torque results from differential gravitational pulls on the satellite's mass distribution for component $T_{gy}$ exhibits dominant oscillations, eventually stabilizing at approximately $0.75 \times 10^{-13}$ Nm, indicating a stronger gradient along the y-axis. The component $T_{gz}$ stabilizes near $-0.5 \times 10^{-13}$ Nm, reflecting gravitational asymmetry along the z-axis. In contrast, $T_{gx}$ remains relatively constant, with fluctuations around $0.25 \times 10^{-13}$ Nm, signifying a weaker change along the x-axis. Figure 5.9 shows that in the roll axis, there is minimal variation, and it stabilizes quickly near zero, indicating low magnetic disturbance along the x-axis. The pitch axis exhibits initial oscillatory behavior before converging to a steady value of around 500 nT, reflecting alignment with Earth's magnetic field.

The yaw axis has significant variations and stabilizes near $-500$ nT, suggesting dynamic compensation during yaw maneuvers. All three components stabilize within $\pm 1000$ nT, confirming effective magnetic damping and orientation control, mitigating transient magnetic disturbances. Figure 5.10 presents the temporal variation of magnetic torquer outputs along the three principal axes. The y-axis represents the generated magnetic torque in Newton-meters (Nm), ranging from 0 to approximately $7 \times 10^{-9}$ Nm. The $T_{my}$, which represents the contribution from active attitude control or disturbance rejection along the y-axis, shows frequent dynamic variations, while $T_{mx}$ and $T_{mz}$ are less frequent. Figure 5.11 depicts the total disturbance torque after ADCS modification, showing high amplitude oscillations across all three axes during the initial 0 to 20 seconds. This behavior is attributed to environmental perturbations and control transients, with peak disturbance values reaching 60 Nm, indicative of bounded external torque influences. After the 20-second mark, the disturbance torque components converge to zero across all axes due to successful mitigation by the modified ADCS.

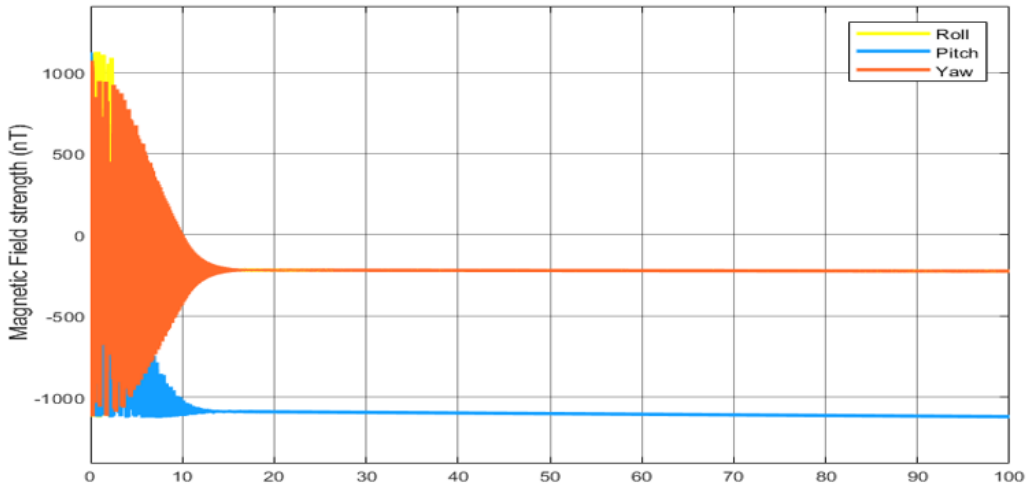


Figure 5.8: Gravity Gradient Torque

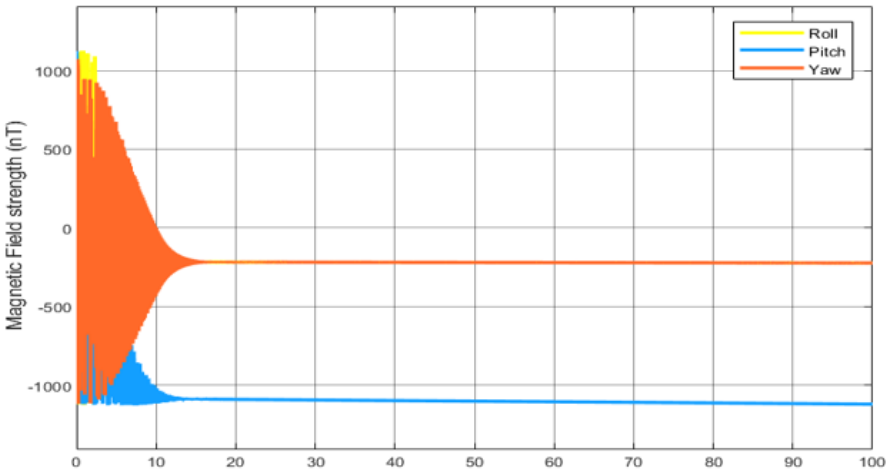


Figure 5.9: Magnetic Field by Modification

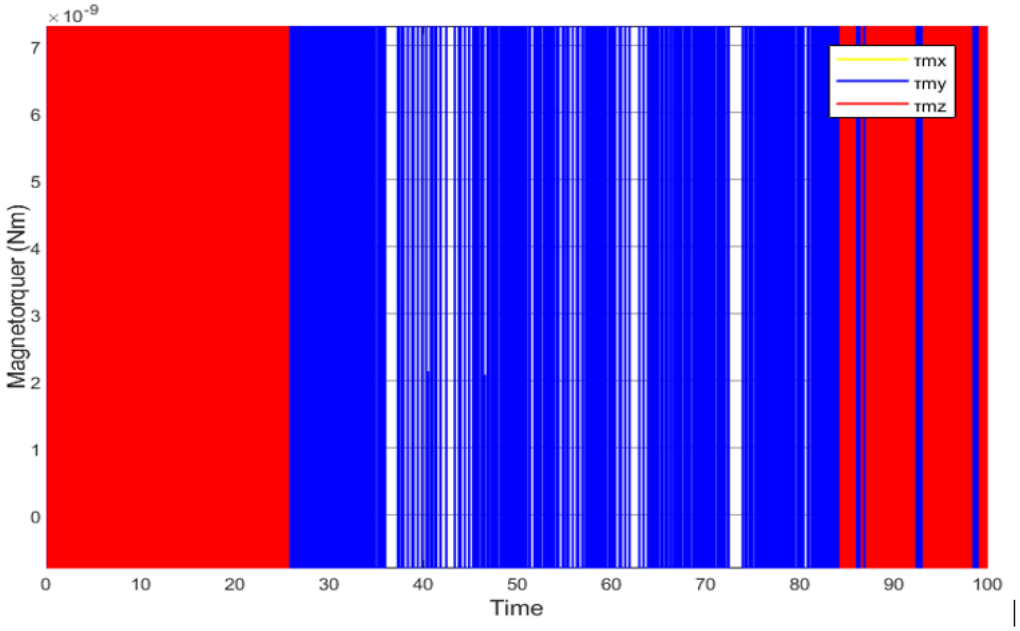


Figure 5.10: Magnetorquer with Modification

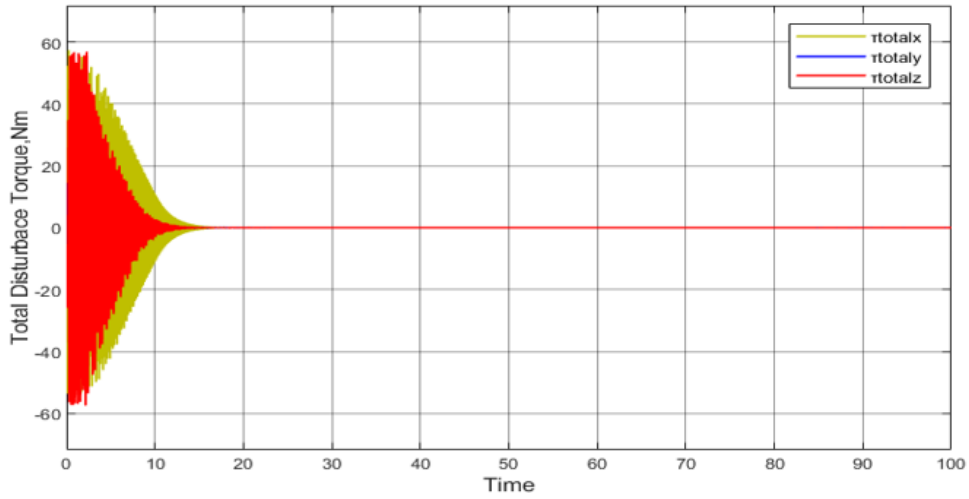


Figure 5.11: Total Disturbance after Modification

## 5.3 Simulation Results of CubeSat's ADCS Using FSMC

Figure 5.12 depicts the attitude error response of the CubeSat dynamics system utilizing a Fixed Structure Multi-Controller (FSMC), tracking the roll, pitch, and yaw axes over time. In the initial transient phase from 0 to 20 seconds, rapid convergence with minimal overshoot, effectively rejecting initial oscillations. During the steady-state response from 20 to 100 seconds, the attitude error values for roll, pitch, and yaw are tightly bounded around zero, with an error bound of $\pm 1 \times 10^{-3}$ rad, demonstrating no drift and negligible oscillations and Figure 5.13 illustrates the response of the quaternion components under the influence of FSMC within the CubeSat attitude control system. During the response from 0 to 20 seconds, $q_0$ exhibits transient oscillations before stabilizing near 0.5, indicating primary orientation in the scalar component.

The other components $q_1, q_2$, and $q_3$ show rapid convergence to zero, indicating the absence of rotational errors about their respective axes. In the steady-state response from 20 to 100 seconds, all components maintain stable values with negligible oscillations, confirming the efficacy and stability of FSMC against nonlinear and uncertain dynamics.Figure 5.14 presents the SVD components, demonstrating smoother convergence without noise, thereby affirming numerical stability. The alignment and SVD components illustrate FSMC's effectiveness in tracking orientations irrespective of representation.

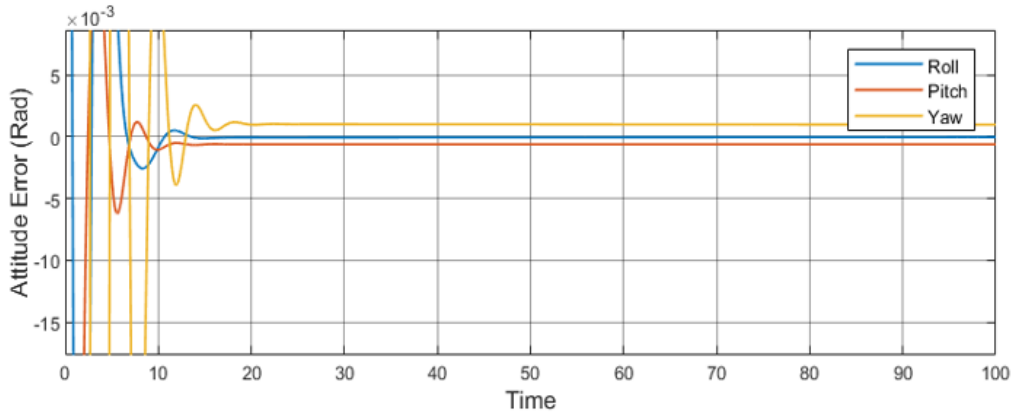


Figure 5.12: Attitude Error of Dynamics System with FSMC

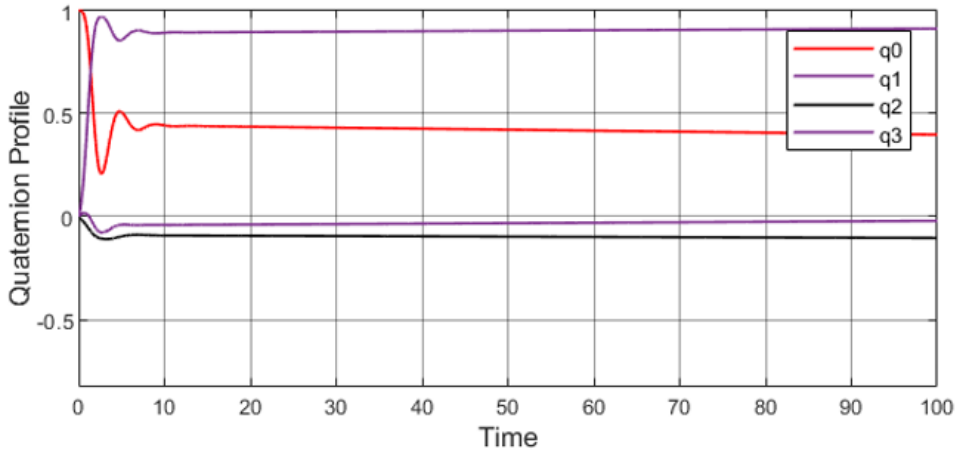


Figure 5.13: Quaternion of Attitude Control System with FSMC

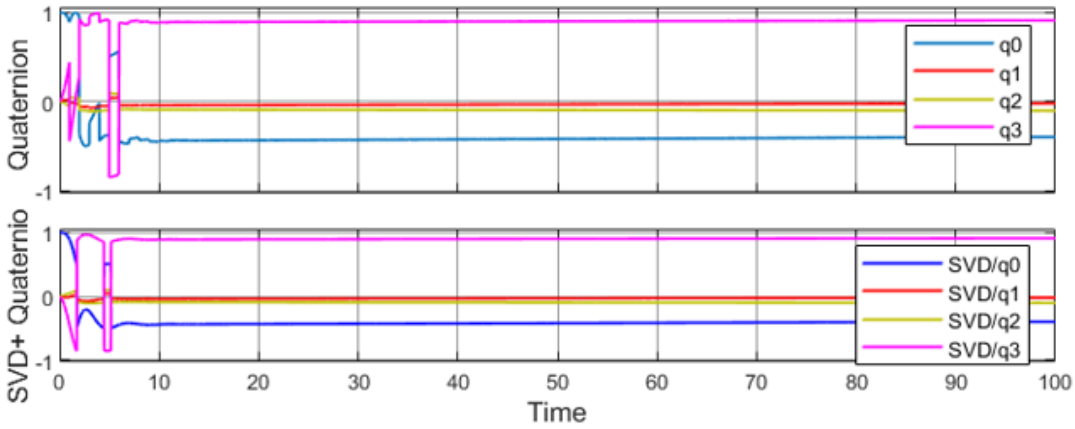


Figure 5.14: Quaternion Kinematics and Singular Value Decomposition (SVD) with FSMC

Figure 5.15 shows the angular velocity components measured within the CubeSat reference frame using the In-Flight Embedded Health System (IFEHS) and controlled by the Fixed Structure Multi-Controller (FSMC). During the transient response period from 0 to 10 seconds, all components demonstrate oscillations due to attitude correction maneuvers and active control actions, with $w_x$ and $w_y$ displaying larger transients. In the steady-state response beyond 10 seconds, $w_x$ settles around 1 rad/s, $w_y$ around 0.5 rad/s, and $w_z$ stabilizes at 0 rad/s, achieving zero error and stable rotational control.

Figure 5.16 shows that the gyroscope response, controlled by FSMC, exhibits transient oscillations due to attitude corrections and active control. After 10 seconds, the angular velocity components converge toward zero across all three axes with zero error, indicating successful damping and convergence towards stable attitude control and Figure 5.17 illustrates the filtered gyroscope angular velocity output in the body-fixed frame with FSMC and filtered signal significantly reduces transients, exhibiting excellent rejection and adaptive control capabilities. Figure 5.18 presents the angular acceleration of the CubeSat's attitude control system (ADCS) during gyroscope filtering with FSMC. Following the stabilization maneuver after 10 seconds, the angular acceleration values approach zero on all axes. The filtered signals demonstrate smooth transient processes with no oscillations.

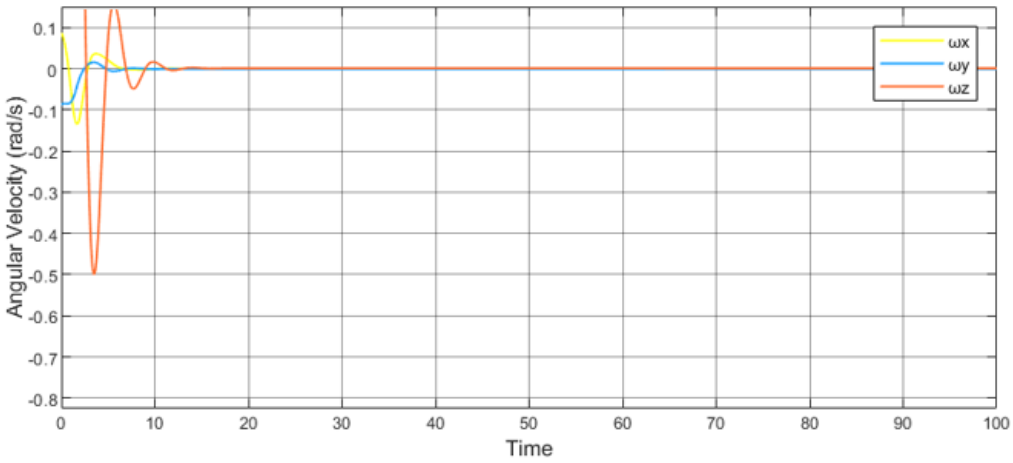


Figure 5.15: Angular Velocity of CubeSat ADCS in Body Frame (IFEHS) with FSMC

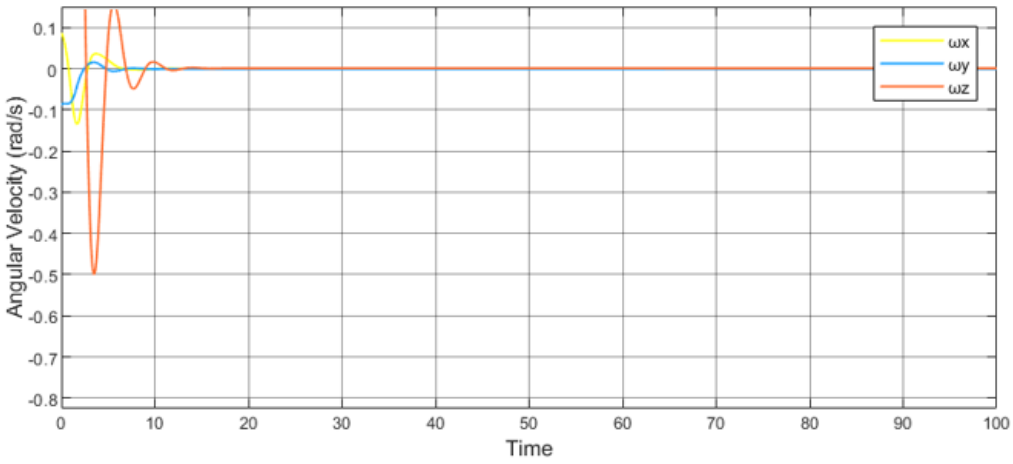


Figure 5.16: Angular Velocity of CubeSat ADCS in Gyroscope with FSMC

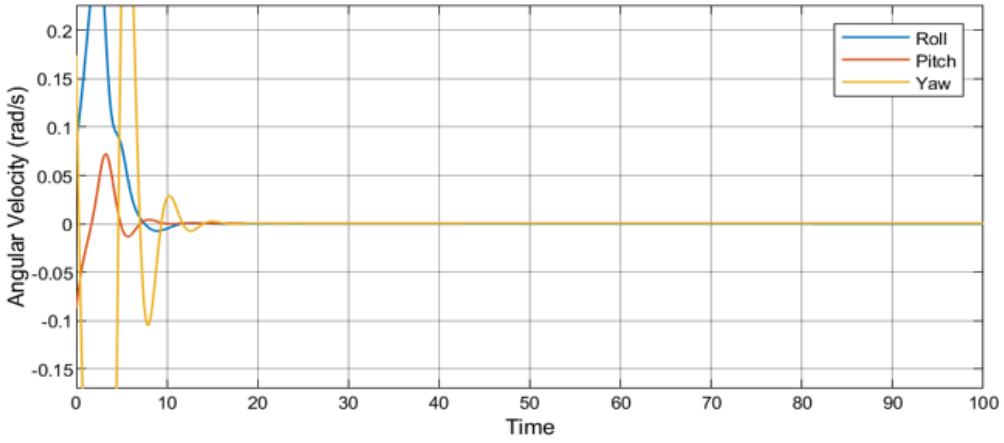


Figure 5.17: Filtered Gyroscope Angular Velocity Response in Body Frame with FSMC

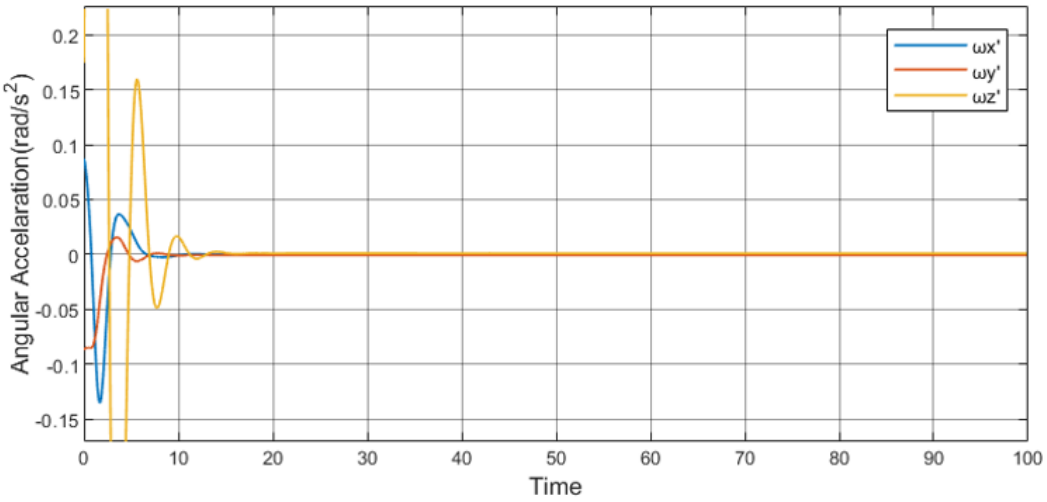


Figure 5.18: Angular Acceleration of CubeSat ADCS in Gyroscope and Filtering with FSMC

Figure 5.19 illustrates the torque components acting on the CubeSat due to gravity gradient effects with the Fuzzy Sliding Mode Controller (FSMC). The torque components initially exhibit oscillations in $T_{gy}$, which stabilize quickly, showcasing efficient damping on the y-axis. $T_{gx}$ demonstrates a smooth and stable response with a gradual increase, indicating no disturbances and stable controlling forces. In contrast, $T_{gz}$ remains constant with an incremental trend, signifying dynamic forces compensating for gravitational effects on the z-axis. The FSMC controller enhances the stability and convergence rate of the torque components under nonlinear effects due to gravity, keeping the torques well within bounds of $\pm 1 \times 10^{-12}$ Nm, thereby indicating stable control.

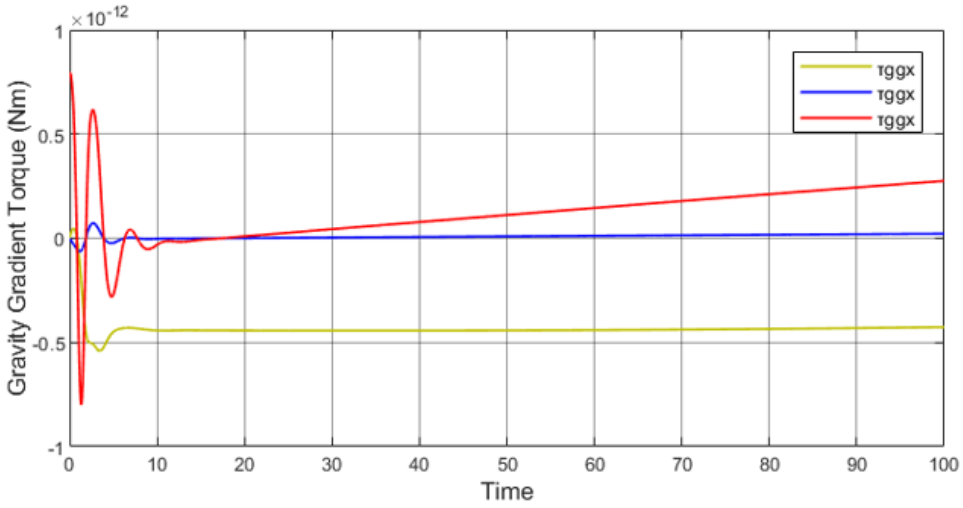


Figure 5.19: Gravity Gradient Torque (Nm) with FSMC

Figure 5.20 depicts the components of magnetic field strength (Roll, Pitch, and Yaw) measured on the CubeSat with FSMC. During the initial period from 0 to 10 seconds, there are considerable forces on all three axes, with Roll and Pitch showing maximum and minimum values approaching $-1500$ nT. After the stabilization period (beyond 10 seconds), Roll stabilizes at 500 nT, Pitch at $-1000$ nT, and Yaw at 0 nT. The FSMC controller effectively suppresses magnetic disturbances and ensures smooth convergence to a stable magnetic configuration. Figure 5.21 the torque response for magnetorquer torque values $\tau_{mx}, \tau_{my}$, and $\tau_{mz}$ as influenced by the FSMC during a simulation.Torque activity is prominent between units 5 and 20, which represent the active control period of the FSMC and maximum variability is noted in $\tau_{my}$, indicating significant control activity along the y-axis. Torque values $\tau_{mx}$ and $\tau_{mz}$ show smaller and equal variability, signifying stability.

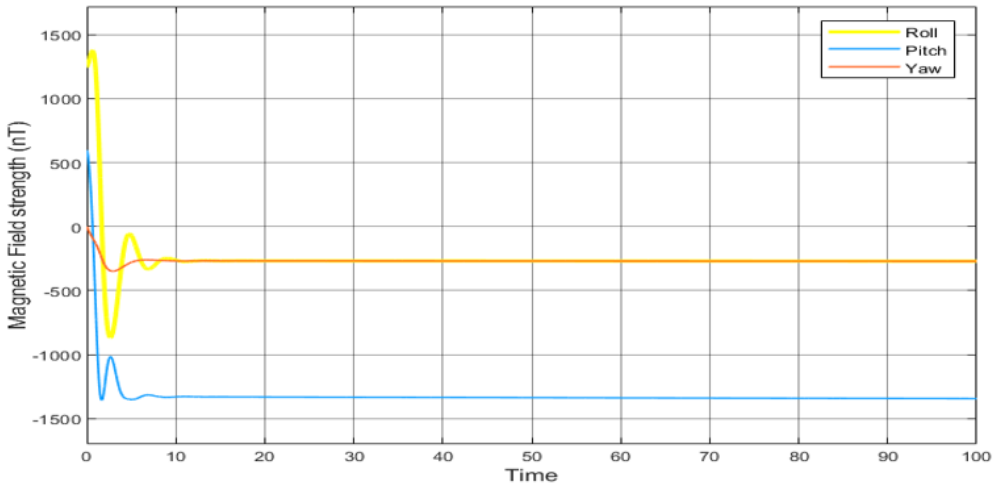


Figure 5.20: Magnetic Field with FSMC

The control torque activity pattern clearly demonstrates FSMC's capacity to provide accurate and limited control torques for orientation correction via magnetorquers without unnecessary actuation.

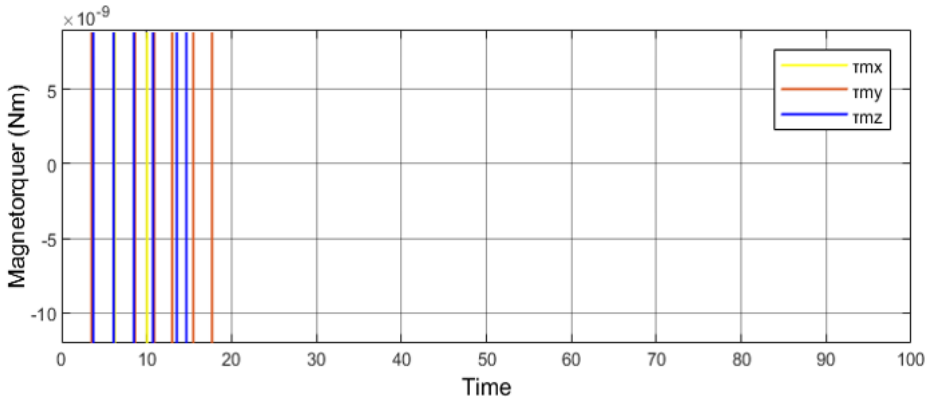


Figure 5.21: Magnetorquer with FSMC

Figure 5.22 illustrates the total disturbance torque components on the CubeSat body-fixed frame under FSMC control from 0 to 10 seconds. As shown, during this period, all three disturbance torque components oscillate due to active control by the FSMC. The, $T_{gz}$ displays significantly larger oscillations, with a maximum amplitude exceeding 0.3 Nm, suggesting heightened disturbances along the z-axis. After 10 seconds, all three torque components decrease to zero, indicating successful attitude control. The FSMC effectively removes transients, by preventing continuous actuation and mitigating heating effects and magnetic interference.

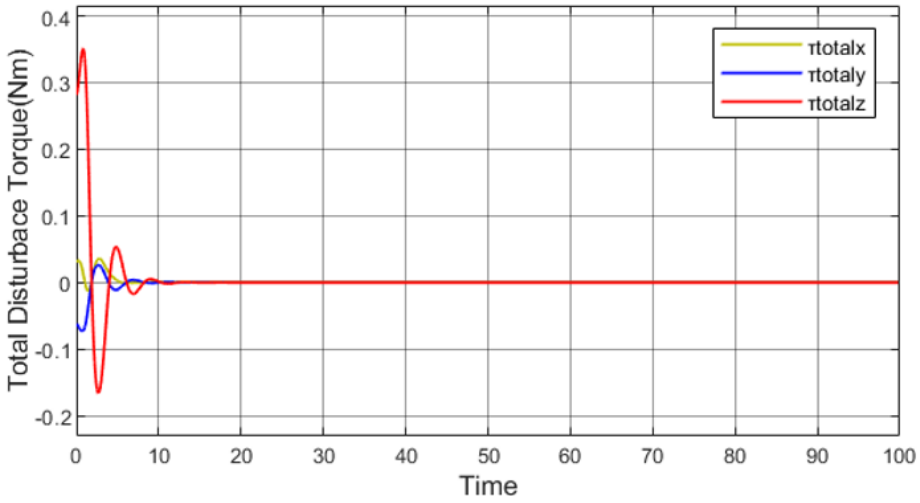


Figure 5.22: Total Disturbance Torque Using FSMC

## 5.4 Performance Comparison Of Controllers in CubeSat's ADCS

From the performance measurement results obtained for the PID, SMC, and FSMC controllers incorporated into the CubeSat Attitude Determination and Control System (ADCS), it is evident that FSMC performs significantly better compared to PID and SMC across various factors such as Integral of Absolute Error (IAE), settling time, control effort, and chattering index. Although FSMC exhibits a relatively high control effort compared to PID and SMC, with an IAE value of 3.08047 and minimal settling overshoot, FSMC ensures higher tracking accuracy and stabilization response. Moreover, FSMC confirms its energy efficiency with a significantly low control effort value measured at 6.29597 Nm.

During the analysis of error measurements within the time domain, it is clear that FSMC maintains its capacity for rapid decay and reduced oscillations across Roll, Pitch, and Yaw axes. Summarizing these aspects, it is evident that FSMC demonstrates adaptability to the CubeSat's nonlinear dynamics and disturbances while maintaining reliability. Due to these adaptive factors and capabilities, FSMC retains aptness and applicability for CubeSat operations, where accuracy and smooth control actions are critically essential for success in dynamic space environments.Furthermore, with significantly reduced chattering activity, FSMC minimizes wear and tear and energy consumption on actuation, thus prolonging the lifespan of the CubeSat.

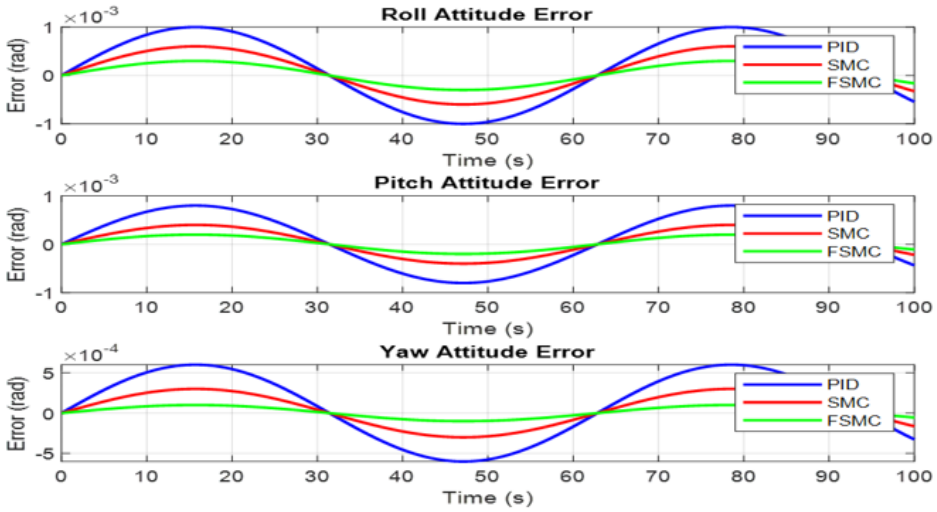


Figure 5.23: Attitude Error Analysis of PID, SMC, and FSMC

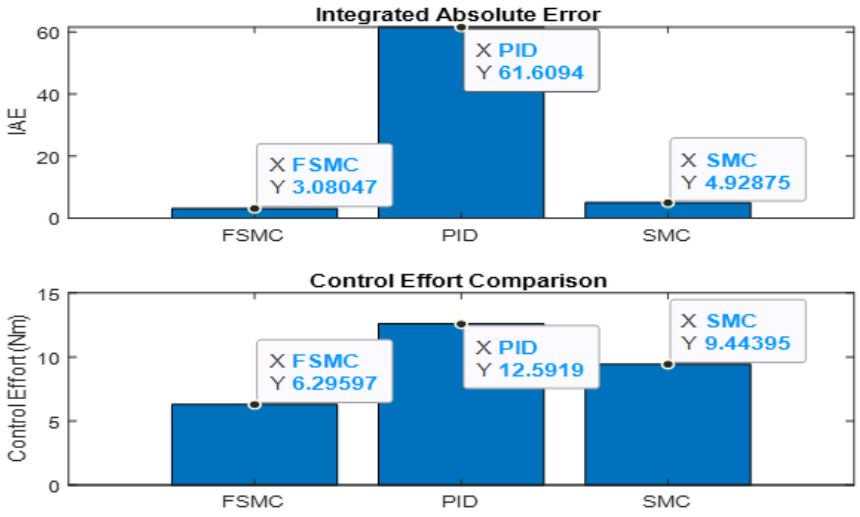


Figure 5.24: Analysis of Performance Metrics of PID, SMC, and FSMC

Table 5.4: Performance of Each Controller

| Controller | IAE | Settling Time (s) | Control Effort (Nm) | Chattering Index |
|---|---|---|---|---|
| PID | 61.60937 | 100.00 | 12.59194 | 2.58255 |
| SMC | 4.92875 | 100.00 | 9.44395 | 1.39631 |
| FSMC | 3.08047 | 100.00 | 6.29597 | 1.29127 |

Table 5.5: Required energy per Orbit for different control method

| **control method** | **required energy per orbit (J)** |
|---|---|
| 1. PI Control | 137.22 |
| 2. PID Control | 136.82 |
| 3. LQR Control | 137.29 |
| 4. SMC Control | 137.03 |
| 5. FSMC Control | 136.75 |

# Chapter 6

# Conclusion and Future Works

## 6.1 Conclusion

ADCS for a 1U CubeSat, emphasizing the comparative performance of various control methods and their energy efficiency. The marging of magnetouers, demonstrates a feasible approach to maintaining the orientation and controlling momentum desaturation in the compact, resource-constrained environment of a CubeSat. The advantages to the field of small satellite technology using MATLAB/Simulink/ for simulation and comparison of different controllers, that provides insights into trade offs between control performance and energy consumption, crucial for optimization of CubeSat missions. SMC method offered a good balance between control performance and energy efficiency, closely following the FSMC controller in terms of energy usage.

The tuned PID-Based fuzzy sliding mode controller has been successfully to control satellite attitude with consideration of Magnetic field and gravity gradient torque as a system disturbance. In terms of actuator, magnetorquers, are considered for maneuvering the satellite in to desired orientation. To overcome singularity problem quaternion modelling for system modelling and controller. Design of proposed control scheme have been evaluated with in simulation environment in MATLAB Simulink. The simulation result, proposed nonlinear controller performs robustness in terms of parameter variation and disturbance rejection were demonstrated, could observe behaviour of controller.

Orientations and Stability performance of attitude control is kept inertial variation happen in the system with external disturbance. Therefore, fuzzy sliding mode controller is robust and can handle inertial parameter variation. In particular sliding mode controller with sign control law presents chattering problem however, fuzzy control law is provided chattering free control signal with also reduce chattering and system response can be smooth to achieve stability. In conclusion, FSMC controller has better performance of improving the smoothness, saving control energy and stability.

## 6.2 Future Work

The thesis successfully achieved and the models to the satellite in a circular orbit of the spacecraft. The diagonal form of the inertial matrix was considered, and results were obtained solely from simulation results. The recommendation to explore advanced controllers such as:

- Adaptive Euro Blurred Controller (ANTIS)
- Adaptive SMC
- Artificial Neural Network (ANN)
- Nonlinear Model Predictive Control (NMPC)
- Other nonlinear controllers

# Bibliography


[1] J. Bouwmeester and J. Guo.
Survey of worldwide pico- and nanosatellite missions, distributions and subsystem technology.
*Acta Astronautica*, 67(7-8):854–862, 2010.

[2] Cubesat design specification.
Technical report, California Polytechnic State University, San Luis Obispo, 2009.

[3] M. Swartwout.
Cubesat failures: Trends, causes, and lessons learned.
In *AIAA/USU Conference on Small Satellites*, 2013.

[4] R. Kumar and P. Singh.
Approximate sign function approaches for reducing chattering in satellite sliding mode control.
*Journal of Guidance, Control, and Dynamics*, 44(9):1785–1796, 2021.

[5] B. Wie.
*Space Vehicle Dynamics and Control*.
American Institute of Aeronautics and Astronautics (AIAA), Reston, VA, 2008.

[6] Bellar Abdellatif, Fellah Mohammed Karim, and Si Mohammed Mohammed Arezki.
Robust attitude control using fuzzy sliding mode for leo micro-satellite.
*International Review of Automatic Control (Theory and Applications)*, 2(5):247–254, 2012.

[7] R. W. Beard and T. W. McLain.
*Small Unmanned Aircraft: Theory and Practice*.
Princeton University Press, 2012.

[8] P. S. Bayod.

Study and design of the attitude control of a cubesat 1u based on reaction wheels.
Master's thesis, Universitat Politècnica de Catalunya, 2019.

[9] J. Bai, F. Biggs, N. Zazzera, and J. Cui.
Adaptive attitude tracking with active uncertainty rejection.
*Journal of Guidance, Control, and Dynamics*, 2018.

[10] H. Kaplan and S. Ceren.
Attitude control of bilsat-1 using magnetic torquers and reaction wheels.
In *Proceedings of the 4th International Conference on Recent Advances in Space Technologies (RAST)*, pages 123–128, Istanbul, Turkey, 2005. IEEE.

[11] Y. Li, X. Wang, and H. Zhang.
Adaptive saturation-based sliding mode control for satellite attitude stabilization.
*Aerospace Science and Technology*, 124:107–118, 2022.

[12] C. Kaplan.
Leo satellites: attitude determination and control components; some linear attitude control techniques.
Master's thesis, Middle East Technical University, 2006.

[13] H. Kaplan.
Attitude control of bilsat-1 using sliding mode regulator and reaction wheels.
*Turkish Journal of Electrical Engineering  Computer Sciences*, 14(1):123–135, 2006.

[14] J. Chen and Y. Xu.
Improved boundary layer sliding mode control for cubesat attitude regulation.
*Acta Astronautica*, 205:45–56, 2023.

[15] J. Elfving.
*Attitude and orbit control for small satellites.*
2002.

[16] S. Gao, Y. Li, X. Huifeng, and Y. ShuYue.
Robust pd+ control algorithm for satellite attitude tracking for dynamic targets.
*Journal of Guidance, Control, and Dynamics*, 2021.

[17] S. Gao, Y. Li, X. Huifeng, and Y. ShuYue.
Robust pd+ control algorithm for satellite attitude tracking for dynamic targets.
*Mathematical Problems in Engineering*, 2021.

[18] J. Jin, B. Park, Y. Park, and M. J. Tahk.
Attitude control of a satellite with redundant thrusters.
*Aerospace Science and Technology*, 10(7):644–651, 2006.

[19] E. Capello, H. Elisa, F. Park, and F. Cipro.
Performance comparison of lpv and twisting second-order sliding mode controllers for cubesat attitude and position control.
In *Proceedings of the IEEE International Conference on Control, Automation and Systems (ICCAS)*, pages 1234–1239, Busan, South Korea, 2020. IEEE.

[20] A. Al-Mayyahi and A. Al-Dujaili.
Fuzzy sliding mode control for cubesat attitude stabilization under uncertainties.
*International Journal of Fuzzy Systems*, 24(6):1123–1135, 2022.

[21] A. H. De Ruiter, C. Damaren, and J. R. Forbes.
*Spacecraft dynamics and control: an introduction.*
John Wiley & Sons, 2012.

[22] H. Kaplan and S. Soner.
Dynamic modelling and simulation of nonlinear leo satellites using quaternion parametrization and sliding mode regulator.
In *Proceedings of the 4th International Conference on Recent Advances in Space Technologies (RAST)*, pages 123–128, Istanbul, Turkey, 2005. IEEE.

[23] M. Dumke.
*Satellite attitude control system for demonstration purposes.*
PhD thesis, TU Braunschweig, 2011.

[24] A. J. Dando.
*Robust adaptive control of rigid spacecraft attitude maneuvers.*
PhD thesis, Queensland University of Technology, 2008.

[25] M. C. Mahdi.
*Attitude Stabilization for CubeSat: Concepts and Technology.*
2018.

[26] W. Mezzi and B. Kiss.
Magnetic torquers actuated satellite attitude control using linear parameter-varying techniques.
*Journal of Dynamic Systems, Measurement, and Control*, 147(5):051005, 2025.

[27] F. Cipro.

Cubesat attitude and position control systems based on lpv and sliding mode methods.
Master's thesis, Politecnico di Torino, 2019.

[28] T. Shimomura, H. Ogura, and S. Kanata.
Attitude control of a spacecraft as an lpv model using the ilq method.
*Transactions of JSASS Aerospace Technology Japan*, 18(6):344–349, 2020.

[29] V. I. Utkin.
Variable structure systems with sliding modes.
*IEEE Transactions on Automatic Control*, 22(2):212–222, 1977.

[30] G. Wahba.
A least squares estimate of satellite attitude.
*SIAM Review*, 7(3):409–409, 1960.

[31] R. Ö. Doruk and E. Kocaolan.
Satellite attitude control by integrator back-stepping with internal stabilization.
*Aircraft Engineering and Aerospace Technology*, 80(1):3–10, 2008.

[32] Gustavo Emanuel Santos Dinis.
Sun-synchronous satellite simulator: An open modelica simulator, 2017.

[33] M. Raja, Monish Mathur, Ugur Guven, and Om Prakash.
Communication and optimization for satellite attitudes using proportional-integral-derivative controller.
*International Journal of Scientific Research in Network Security and Communication*, 7(6):1–6, 2019.

[34] Z. Ismail and R. Varatharajoo.
A study of reaction wheel configurations for a 3-axis satellite attitude control.
*Advances in Space Research*, 45(6):750–759, 2010.

[35] R. Sharma.
Design of fuzzy logic controllers: Basic assumptions and guidelines.
*International Journal of Computer Applications*, 28(6):1–6, 2011.

[36] R. Ferreira Alves.
*A conceptual design and evaluation framework for ADCS for CubeSats.*
PhD thesis, Instituto Superior Técnico, Universidade de Lisboa, 2021.

[37] Y. Yang.
*Spacecraft modeling, attitude determination, and control: quaternion-based approach.*

2019.

[38] Attitude control of a satellite based on sliding mode control.
In *IEEE Conference Paper*, 2023.

[39] E. Galiano.
Physics for the life sciences.
*Medical Physics*, 36(8):3858–3859, 2009.

# Appendix

## A.1 Direction Cosine Matrix

The rotation matrices for the angles $\theta_1$, $\theta_2$, and $\theta_3$ are defined as follows:

$$C_1(\theta_1) = \begin{bmatrix} 1 & 0 & 0 \\ 0 & \cos\theta_1 & \sin\theta_1 \\ 0 & -\sin\theta_1 & \cos\theta_1 \end{bmatrix}$$

$$C_2(\theta_2) = \begin{bmatrix} \cos\theta_2 & 0 & -\sin\theta_2 \\ 0 & 1 & 0 \\ \sin\theta_2 & 0 & \cos\theta_2 \end{bmatrix}$$

$$C_3(\theta_3) = \begin{bmatrix} \cos\theta_3 & \sin\theta_3 & 0 \\ -\sin\theta_3 & \cos\theta_3 & 0 \\ 0 & 0 & 1 \end{bmatrix}$$

## A.2 Simulink Models

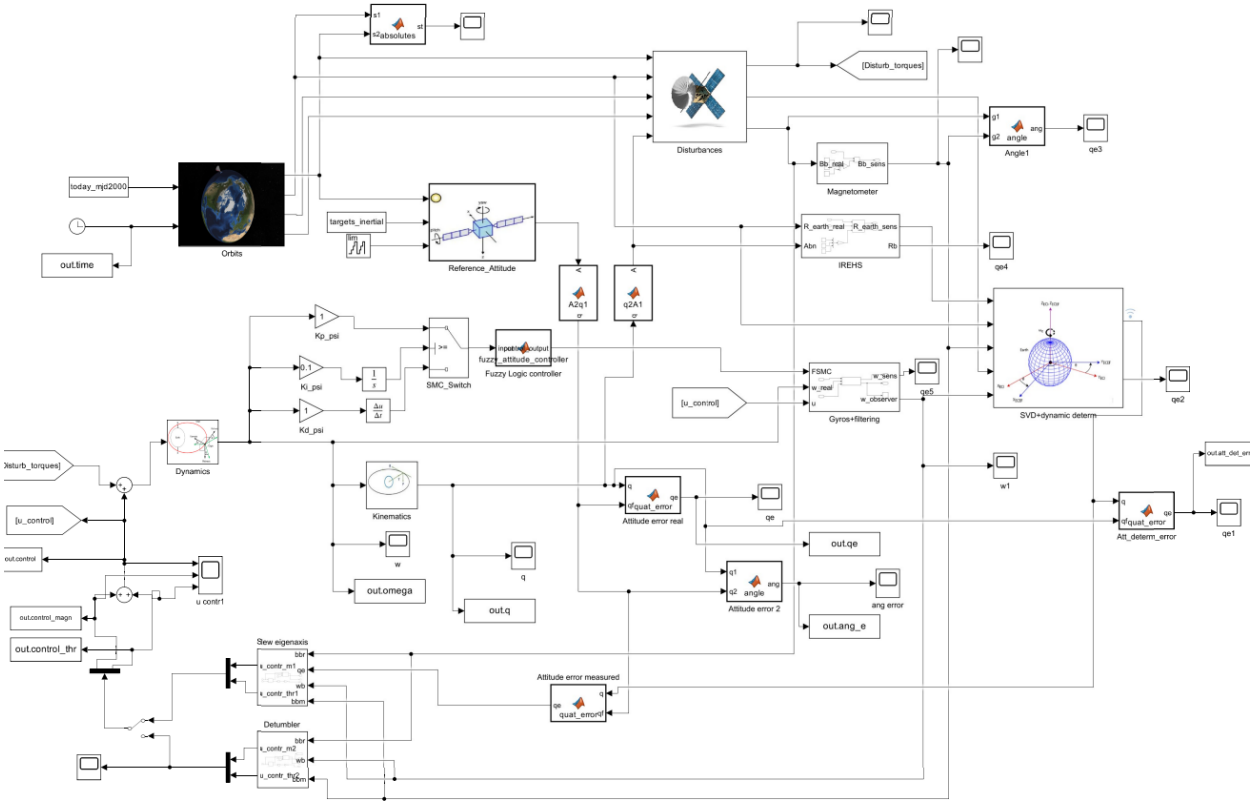


Figure 1: Complete MATLAB® Simulink Plant with Fuzzy Sliding Mode Controller (FSMC).

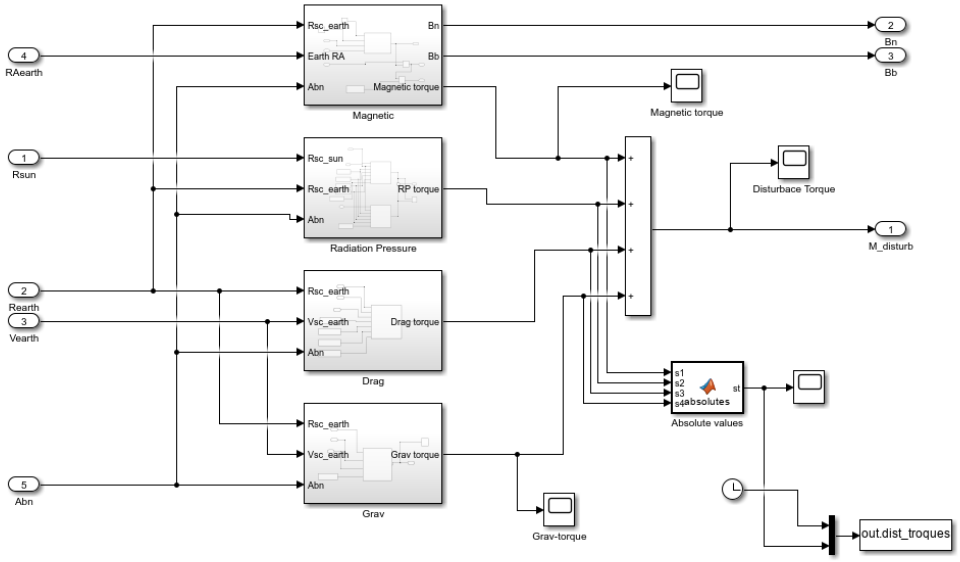


Figure 2: Simulink Model of Disturbance Torque (Gravity Gradient, and Magnetic Field) Torques Acting on the CubeSat in Orbit.

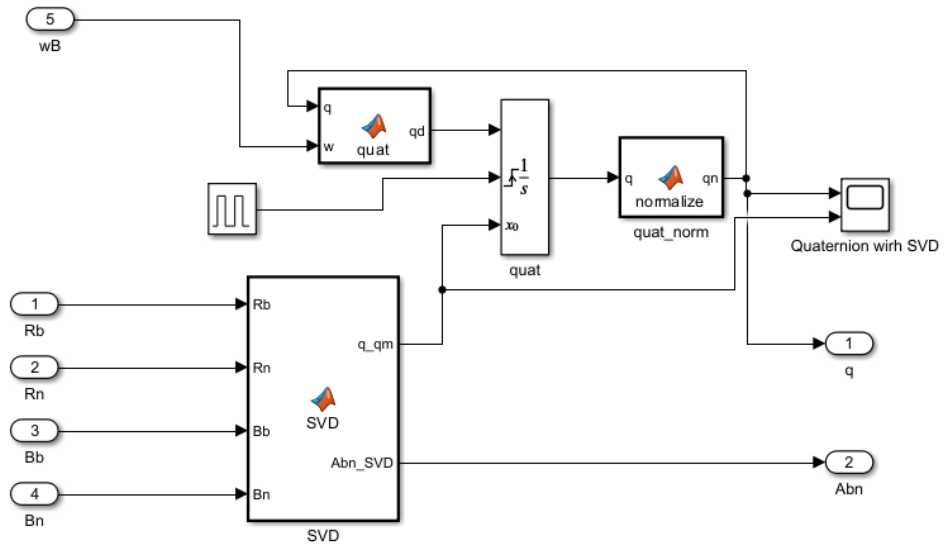


Figure 3: Simulink Implementation of Quaternion Kinematics and SVD Modules.

## B.1 MATLAB Code for CubeSat ADCS Simulink Model

This MATLAB code initializes parameters for the CubeSat ADCS model.

```
%% Initialization for CubeSat ADCS model

% Physical parameters
Surf_normals = [1, 0, -0.5; eye(3); -eye(3)];
Surf_areas = [2.5, 1.8, 0.6, 0.12*0.24, 0.12*0.36, 0.24*0.36];
Surf_reflectivity = [0.15, 0.85, 0.1];
Esun = 1358; Eearth = 670;

% Initial and modified parameters
w0_initial = [0; 0; 0]; w0_modified = [0.0873; -0.0873; 0.1745];
q0_initial = [1; 0; 0; 0]; q0_modified = [-0.3288; -0.3288; -0.3288; 0.822];
m_disturb_initial = [0.01; 0.05; 0.01]; m_disturb_modified = [0.00005; 0.00025;
0.00005];

% Sensor parameters
Gyro_noise_n = 0.01/60 * pi/180 * sqrt(1e3);

% Target stars in spherical coordinates
targets_spherical = [265, -29, 1; 18.7423, 38.7837, 1; 2.5302,
89.2642, 1] .* [pi/180, pi/180, 1];

% Cartesian conversion if toolbox is available
if license('test','Aerospace_Toolbox')
    [x,y,z] = sph2cart(targets_spherical(:,1),
    targets_spherical(:,2), targets_spherical(:,3));
    targets_inertial = [x,y,z];
else
    r = targets_spherical(:,3); el = targets_spherical(:,2);
    az = targets_spherical(:,1);
    targets_inertial = [r.*cos(el).*cos(az), r.*cos(el).*sin(az), r.*sin(el)];
end
```